CD26-mediated co-stimulation in CD8$^+$ T cells preferentially enhances excretion of GzmB as compared with CD28-mediated co-stimulation

The data above suggest that CD26$^+$ CD8$^+$ T cells have a different effector role from CD28$^+$ CD8$^+$ T cells. To examine the cellular function associated with each co-stimulatory effect, we performed co-stimulation studies using anti-CD3 and/or anti-CD26 or anti-CD28 mAbs. For this purpose, we first performed a cell proliferation assay. As shown in the Supplementary data section, neither whole T cells (pan-T cells) of human PBMC nor purified CD8$^+$ T cells exhibited proliferative activity following stimulation with anti-CD3 mAb alone (see Supplementary material, Fig. S1), whereas both pan-T cells and CD8$^+$ T cells showed equal enhancement of proliferation by anti-CD3 plus anti-CD28 or anti-CD3 plus anti-CD26 co-stimulation (Fig. S1a,b). These data indicate that CD8$^+$ T cells exhibit proliferative activity through either CD26-mediated or CD28-mediated co-stimulation. We next examined production of cytotoxic granules or cytokines in the presence of CD26-mediated or CD28-mediated co-stimulation. For this purpose, we evaluated the expression levels of PRF, GzmA or GzmB in CD8$^+$ T cells. As shown in Fig. 3(a), expression of GzmB in CD8$^+$ T cells was increased following CD26-mediated co-stimulation compared with CD28-mediated co-stimulation at any stimulation intensity (Fig. 3a). Moreover, time–course analysis showed that GzmB expression was greater over the tested time intervals after CD26-mediated co-stimulation than after CD28-mediated co-stimulation (Fig. 3b). In contrast, no difference in the expression of PRF or GzmA was observed following CD26-mediated co-stimulation or CD28-mediated co-stimulation (data not shown).

To confirm the differences in effector function associated with CD26-mediated co-stimulation in CD26^{high} CD8$^+$ T cells from that of CD26^{int} CD8$^+$ T cells, we examined the expression of GzmB in CD8$^+$ T cells following purification by anti-CD26 mAb and anti-mouse IgG$_1$ microbeads. As shown in the Supplementary material, Fig. S2, both CD26^{high} CD8$^+$ and CD26^{int} CD8$^+$ cells were selected in the positive fraction after purification (Fig. S2b), whereas CD26^{int} CD8$^+$ and CD26$^-$ CD8$^+$ cells were contained in the flow-through (negative fraction) (Fig. S2c). Using each positive or

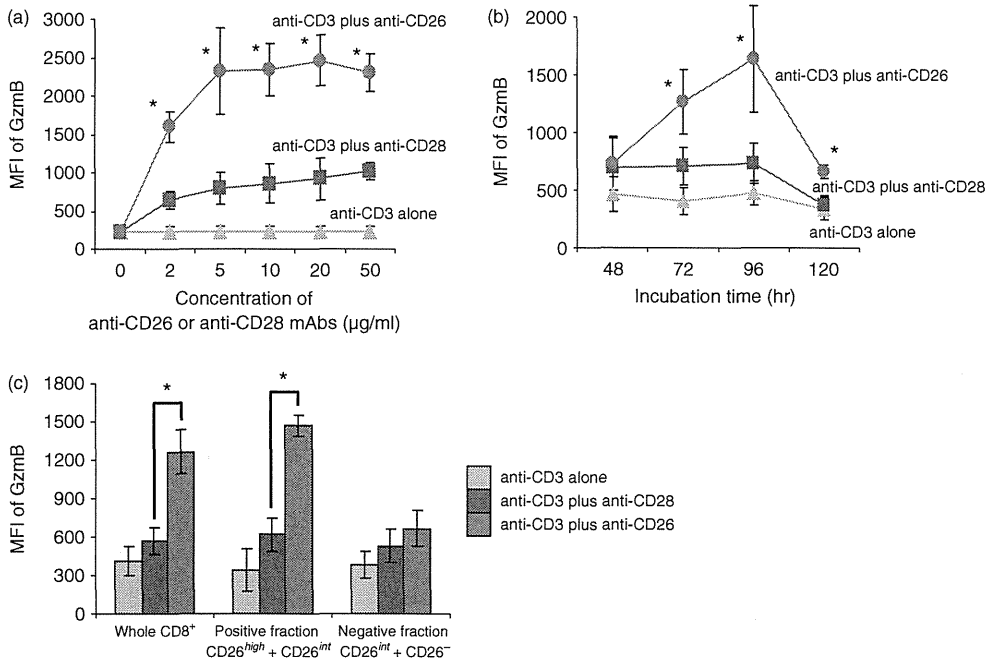

Figure 3. CD26-mediated co-stimulation of CD8$^+$ T cells induces greater Granzyme B expression than CD28-mediated co-stimulation. (a) Purified CD8$^+$ T cells were stimulated with anti-CD3 monoclonal antibodies (mAb) alone, anti-CD3 plus anti-CD28 mAbs, or anti-CD3 plus anti-CD26 mAbs at the indicated concentrations for 72 hr. (b) Purified CD8$^+$ T cells were stimulated with anti-CD3 mAb alone, anti-CD3 plus anti-CD28 mAbs (5 μg/ml), or anti-CD3 plus anti-CD26 mAbs (5 μg/ml) for the indicated time. (c) Purified CD8$^+$ T cells were separated using anti-CD26 mAb (5F8) and anti-mouse IgG$_1$-conjugated magnetic beads as described in the Materials and methods. Whole CD8$^+$ T cells, positively selected cells (positive fraction) or negatively selected cells (negative fraction) were stimulated and incubated by the same method as shown in (b) for 72 hr. Intracellular granzyme B (GzmB) was detected by flow cytometry. Data are shown as mean ± SE of mean fluorescence intensity (MFI) of GzmB from two independent donors (a) and five independent donors (b,c), comparing MFI in anti-CD3 plus anti-CD26 to that in anti-CD3 plus anti-CD28 (*$P < 0{\cdot}01$).

negative fraction, expression of GzmB following CD26 or CD28 co-stimulation was analysed. As shown in Fig. 3(c), GzmB was equally expressed in cells of the negative fraction ($CD26^{int}$ $CD8^+$ and $CD26^-$ $CD8^+$ cells) either by CD26 co-stimulation or by CD28 co-stimulation. On the other hand, in the positive fraction (mixture of $CD26^{high}$ $CD8^+$ and $CD26^{int}$ $CD8^+$ cells), GzmB expression was much more enhanced by CD26-mediated co-stimulation than by CD28-mediated co-stimulation (* in Fig. 3c). These observations strongly suggest that the $CD26^{high}$ $CD8^+$ subset, but not the $CD26^{int}$ $CD8^+$ subset, is essential to induce distinctive CD26-mediated effector function from CD28-mediated co-stimulation.

In addition to increased GzmB expression, production of TNF-α, IFN-γ and sFasL in $CD8^+$ T cells was greater following CD26 co-stimulation than CD28 co-stimulation (Fig. 4a-i–iii). In contrast with these inflammatory cytokines, production of IL-2 by $CD8^+$ T cells was apparently less following CD26 co-stimulation than the level seen with CD28 co-stimulation (Fig. 4a-iv). The same effect was also found on the cytokine production over a wide range of anti-CD26 and anti-CD28 mAbs tested as well as the induction of GzmB expression (data not shown). To confirm the above results regarding cytokine production, we conducted real-time RT-PCR. As shown in Fig. 4(b), mRNA expression of TNF-α, IFN-γ or IL-2 (but not FasL) was significantly up-regulated following CD28

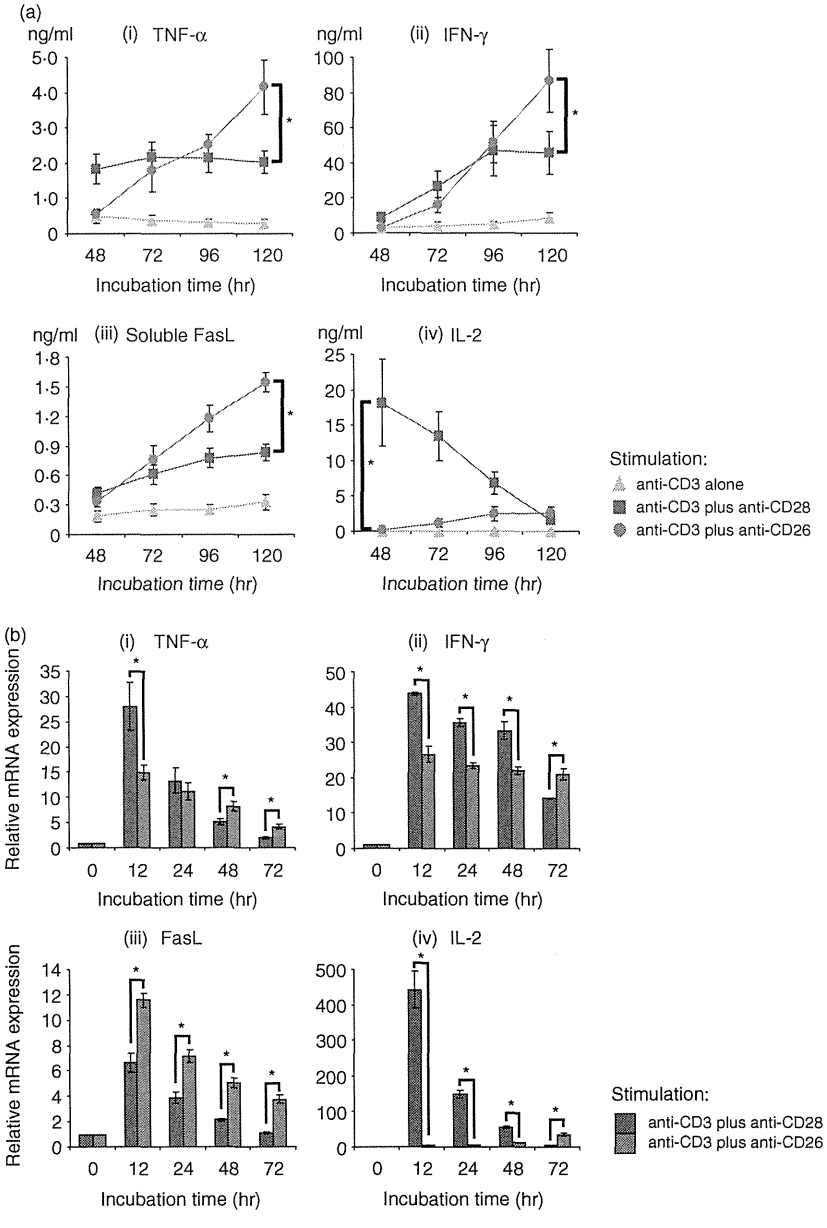

Figure 4. CD26-mediated co-stimulation of $CD8^+$ T cells induces greater levels of tumour necrosis factor-α (TNF-α), interferon-γ (IFN-γ), and soluble Fas ligand (sFasL) than CD28-mediated co-stimulation. Purified $CD8^+$ T cells were stimulated with anti-CD3 monoclonal antibody (mAb) alone, anti-CD3 plus anti-CD28 mAbs, or anti-CD3 plus anti-CD26 mAbs for the indicated times. (a) Concentrations of TNF-α (i), IFN-γ (ii), sFasL (iii) and interleukin-2 (IL-2) (iv) were examined by ELISA. (b) mRNA expression of TNF-α (i), IFN-γ (ii), FasL (iii) and IL-2 (iv) was quantified by real-time RT-PCR. Each expression was normalized to HPRT1 and relative expression levels compared with resting $CD8^+$ T cells (0 hr) were shown. Data are shown as mean ± SE of triplicate wells from six independent donors (a) and shown as mean ± SD of triplicate samples (b), comparing values in anti-CD3 plus anti-CD26 to that in anti-CD3 plus anti-CD28 (*$P < 0.01$).

co-stimulation compared with CD26 co-stimulation at the 12 hr incubation time period. Meanwhile, mRNA expression levels of all the cytokines tested were higher after 72 hr of CD26 co-stimulation than CD28 co-stimulation (Fig. 4b-i–iv). These results correlated with the kinetics of cytokine production shown in Fig. 4(a). Taken together, these data suggest that CD26 co-stimulation results in enhanced $CD8^+$ T-cell effector function by increasing production of GzmB, TNF-α, IFN-γ or sFasL, compared with CD28 co-stimulation.

CD26-mediated co-stimulation of $CD8^+$ T cells preferentially enhances cytotoxic effect compared with CD28-mediated co-stimulation

Finally, we conducted cytotoxic assays by mixed lymphocyte reaction (MLR) in the presence of CD26-mediated or CD28-mediated co-stimulation. For this purpose, CFSE-labelled U937 cells were co-cultured with activated $CD8^+$ T cells, and then cells were harvested and stained with Annexin V-PE and 7-AAD. CFSE-positive cells (U937) as target cells were gated in to detect Annexin V^+ 7-AAD^+ dead cells (see Supplementary material, Fig. S3a). As shown in Fig. 5, higher levels of Annexin V^+ 7-AAD^+ cells were found by CD26-mediated cytotoxic effect than by CD28-mediated effect (* in Fig. 5). This cytotoxic effect of $CD8^+$ T cells induced by CD26-mediated co-stimulation was enhanced with increasing levels of effector cells in a dose-dependent manner (Fig. 5). Moreover, this cytotoxic effect via CD26-mediated co-stimulation was significantly decreased by GzmB inhibitor or anti-FasL neutralizing antibody (Fig. S3b). These data strongly suggest that CD26-mediated co-stimulation is sufficient to induce cytotoxic effector function in $CD8^+$ T cells via GzmB and/or FasL and that the CD26 pathway of co-stimulation is distinctive from the CD28 pathway.

Discussion

In the present study, we demonstrate that $CD26^{high}$ $CD8^+$ T cells belong to an early EM subset and that the cytotoxic effect of human $CD8^+$ T cells is exerted in part by CD26-mediated co-stimulation of $CD26^{high}$ $CD8^+$ T cells, resulting in enhanced expression of GzmB, TNF-α, IFN-γ and sFasL.[12–14]

Analysis of cell surface markers and intracellular cytotoxic granules indicates that $CD26^{high}$ $CD8^+$ T cells exclusively express CD28 and belong to an early EM subset (Figs 1 and 2). In fact, CD26-mediated co-stimulation of $CD26^{high}$ $CD8^+$ T cells induced increased expression levels of GzmB, TNF-α, IFN-γ and sFasL, as well as enhanced cytotoxic effect (Figs 3, 4 and 5). Of note is that CD26-mediated co-stimulation resulted in greater effector function than that induced by CD28-mediated co-stimulation. These findings strongly suggest that the CD26 co-stimulation pathway in $CD8^+$ T cells resulting in enhanced cytotoxic effect is distinct from the CD28 co-stimulation pathway. In contrast to $CD26^{high}$ $CD8^+$ T cells, $CD26^{int}$ $CD8^+$ T cells belong to the naive subset (Figs 1 and 2). Moreover, co-stimulation through either the CD26 or CD28 pathway did not result in differences in effector function of $CD26^{int}$ $CD8^+$ T cells (Fig. 3). Purification of $CD26^{high}$ $CD8^+$ and $CD26^{int}$ $CD8^+$ T cells by cell sorting may be required for more precise analyses of effector function of these two subsets instead of using the MACS separation system.

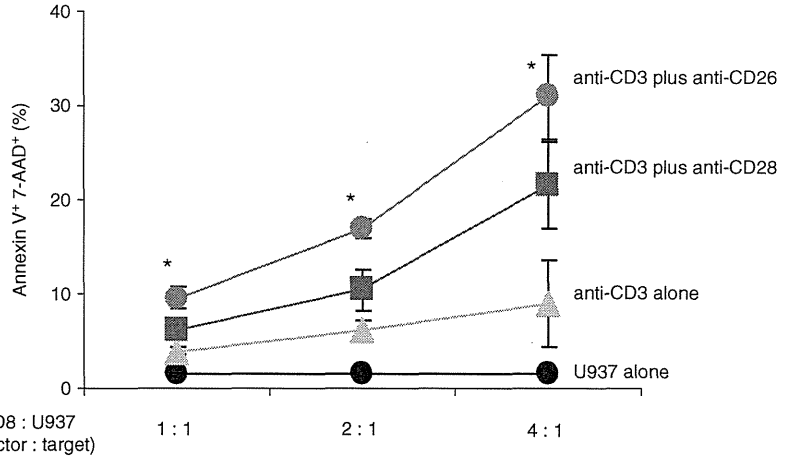

Figure 5. CD26-mediated co-stimulation of $CD8^+$ T cells results in greater cytotoxic effect than CD28-mediated co-stimulation. Stimulated $CD8^+$ T cells and CFSE-labelled U937 cells were used as effector and target cells, respectively. Mixed lymphocyte reaction assay using these effector and target cells was conducted as described in Materials and methods. Data are shown as mean ± SE of % positive cells stained with Annexin V and 7-AAD among CFSE-positive cells (U937 target cells) from four independent donors, comparing percentage of positive cells in anti-CD3 plus anti-CD26 to that in anti-CD3 plus anti-CD28 (*$P < 0{\cdot}01$).

The expression pattern of cytotoxic granules or cytokines in $CD8^+$ T cells induced by CD26-mediated co-stimulation was clearly distinct from that induced by CD28-mediated co-stimulation. As shown in Figs 3 and 4, GzmB (Fig. 3), TNF-α (Fig. 4a-i), IFN-γ (Fig. 4a-ii) and sFasL (Fig. 4a-iii) levels were higher in CD26-stimulated $CD8^+$ T cells than in CD28-stimulated $CD8^+$ T cells. Moreover, CD26-mediated co-stimulation resulted in greater cytotoxic effect as analysed by MLR assays than CD28-mediated co-stimulation (Fig. 5). These results may be partly because the $CD28^+$ subset in $CD8^+$ T cells is composed of heterogeneous cell populations, whereas the $CD26^+$ $CD8^+$ T cells only consist of an early EM ($CD26^{high}$) and a naive ($CD26^{int}$) subset (Figs 1 and 2). Besides differences in cytotoxic effect, IL-2 production in $CD8^+$ T cells was also different in CD26-mediated co-stimulation compared with CD28-mediated co-stimulation (Fig. 4a-iv). Lower production of IL-2 induced by CD26-mediated co-stimulation may produce lower proliferative activity in early phase as shown in Fig. S1 (* at 72 hr). Our present data therefore support the notion that the signalling pathway via CD26 is distinct from signalling induced through the CD28 molecule, as we have previously demonstrated in human $CD4^+$ T cells,[15,16] although the exact mechanisms involved remain to be elucidated.

Taken together, our present findings strongly suggest that $CD26^{high}$ $CD8^+$ T cells have a distinctive effector function in humans, and that the CD26-mediated co-stimulation pathway is different from that of CD28. In this regard, $CD26^{high}$ $CD8^+$ T cells may have a key role in acquired immune reactions such as antigen-specific host defence against infection or cancer, and the pathophysiology of autoimmune diseases or transplantation-related immune disorders such as graft-versus-host disease or graft rejection. Therefore, targeting $CD26^{high}$ $CD8^+$ T cells has the potential to be useful in studies of immune responses to new vaccine candidates as well as innovative therapies for immune-mediated diseases.

Acknowledgements

This work was supported by Grant-in-Aid from the Ministry of Education, Science, Sports and Culture (K.O. and C.M.) and the Ministry of Health, Labour and Welfare, (C.M.) Japan.

Conflicts of interests

None.

Disclosure

None.

References

1 Morimoto C, Schlossman SF. The structure and function of CD26 in the T-cell immune response. *Immunol Rev* 1998; **161**:55–70.
2 Morimoto C, Torimoto Y, Levinson G, Rudd CE, Schrieber M, Dang NH, Letvin NL, Schlossman SF. 1F7, a novel cell surface molecule, involved in helper function of CD4 cells. *J Immunol* 1989; **143**:3430–9.
3 Ohnuma K, Munakata Y, Ishii T *et al.* Soluble CD26/dipeptidyl peptidase IV induces T cell proliferation through CD86 up-regulation on APCs. *J Immunol* 2001; **167**: 6745–55.
4 Ohnuma K, Yamochi T, Uchiyama M *et al.* CD26 up-regulates expression of CD86 on antigen-presenting cells by means of caveolin-1. *Proc Natl Acad Sci USA* 2004; **101**:14186–91.
5 Ohnuma K, Yamochi T, Uchiyama M *et al.* CD26 mediates dissociation of Tollip and IRAK-1 from caveolin-1 and induces upregulation of CD86 on antigen-presenting cells. *Mol Cell Biol* 2005; **25**:7743–57.
6 Ohnuma K, Uchiyama M, Yamochi T *et al.* Caveolin-1 triggers T-cell activation via CD26 in association with CARMA1. *J Biol Chem* 2007; **282**:10117–31.
7 Ibegbu CC, Xu YX, Fillos D, Radziewicz H, Grakoui A, Kourtis AP. Differential expression of CD26 on virus-specific $CD8^+$ T cells during active, latent and resolved infection. *Immunology* 2009; **126**:346–53.
8 Matteucci E, Ghimenti M, Di Beo S, Giampietro O. Altered proportions of naive, central memory and terminally differentiated central memory subsets among $CD4^+$ and $CD8^+$ T cells expressing CD26 in patients with type 1 diabetes. *J Clin Immunol* 2011; **31**:977–84.
9 Torimoto Y, Dang NH, Tanaka T, Prado C, Schlossman SF, Morimoto C. Biochemical characterization of CD26 (dipeptidyl peptidase IV): functional comparison of distinct epitopes recognized by various anti-CD26 monoclonal antibodies. *Mol Immunol* 1992; **29**:183–92.
10 Sallusto F, Lenig D, Forster R, Lipp M, Lanzavecchia A. Two subsets of memory T lymphocytes with distinct homing potentials and effector functions. *Nature* 1999; **401**:708–12.
11 Takata H, Takiguchi M. Three memory subsets of human $CD8^+$ T cells differently expressing three cytolytic effector molecules. *J Immunol* 2006; **177**:4330–40.
12 Medema JP, Toes RE, Scaffidi C *et al.* Cleavage of FLICE (caspase-8) by granzyme B during cytotoxic T lymphocyte-induced apoptosis. *Eur J Immunol* 1997; **27**:3492–8.
13 Scaffidi C, Fulda S, Srinivasan A *et al.* Two CD95 (APO-1/Fas) signaling pathways. *EMBO J* 1998; **17**:1675–87.
14 Croft M. The role of TNF superfamily members in T-cell function and diseases. *Nat Rev Immunol* 2009; **9**:271–85.
15 Ohnuma K, Takahashi N, Yamochi T, Hosono O, Dang NH, Morimoto C. Role of CD26/dipeptidyl peptidase IV in human T cell activation and function. *Front Biosci* 2008; **13**:2299–310.
16 Ohnuma K, Dang NH, Morimoto C. Revisiting an old acquaintance: CD26 and its molecular mechanisms in T cell function. *Trends in Immunol* 2008; **29**:295–301.

Supporting Information

Additional Supporting Information may be found in the online version of this article:

Figure S1. CD26-mediated co-stimulation or CD28-mediated co-stimulation equally enhances proliferation of $CD8^+$ T cells as well as $CD3^+$ T cells.

Figure S2. CD26 expression of $CD8^+$ T cells following isolation by anti-human CD26 monoclonal antibody-conjugated magnetic beads.

Figure S3. CD26-mediated co-stimulation enhances cytotoxic function of $CD8^+$ T cells as analysed by mixed lymphocyte reaction assays.

CD9 expression as a favorable prognostic marker for patients with malignant mesothelioma

VISHWA JEET AMATYA[1], YUKIO TAKESHIMA[1], KEISUKE AOE[2], NOBUKAZU FUJIMOTO[3], TOSHIHIRO OKAMOTO[4], TAKETO YAMADA[5], TAKUMI KISHIMOTO[3], CHIKAO MORIMOTO[4] and KOUKI INAI[1]

[1]Department of Pathology, Institute of Biomedical and Health Sciences, Hiroshima University, Hiroshima; [2]Department of Medical Oncology, Yamaguchi-Ube Medical Center, Yamaguchi; [3]Department of Respiratory Medicine, Okayama Rosai Hospital, Okayama; [4]Division of Clinical Immunology, Advanced Clinical Research Center, Institute of Medical Science, University of Tokyo, Tokyo; [5]Department of Pathology, Keio University, Tokyo, Japan

Received August 23, 2012; Accepted October 2, 2012

DOI: 10.3892/or.2012.2116

Abstract. CD9 is involved in cell growth, adhesion and motility and its expression is reported to be of prognostic significance in various types of human malignancies. We found increased cell migration in the mesothelioma cell lines MSTO-211H and TUM1 following *in vitro* shRNA-mediated knockdown of CD9 expression. We investigated CD9 expression in 112 malignant pleural mesotheliomas. CD9 expression was observed in 62 of 71 epithelioid, 13 of 20 biphasic and only 1 of 21 sarcomatoid mesotheliomas. Among the epithelioid mesotheliomas (EMs), CD9 expression was observed in all of the 33 cases with a differentiated type (EM-D) and in 29 of the 38 cases with a less-differentiated type (EM-LD). Patients with CD9 expression showed higher 1- and 2-year survival rates (63 and 25%) compared to the patients without CD9 expression (39 and 11%). Univariate analysis revealed that patients with CD9 expression demonstrated a more favorable survival (P=0.0025) along with other clinicopathological factors, including age younger than 60 years, IMIG stage I-II, epithelioid histology, EM-D and patients who underwent extrapleural pneumonectomy or received chemotherapy. Multivariate analysis identified CD9 expression as an independent prognostic factor with a hazard ratio (HR) of 1.99 in the analysis of all mesotheliomas (P=0.0261) and an HR of 2.60 in the analysis of EMs (P=0.0376). CD9 expression is an independent favorable prognostic marker of malignant mesothelioma.

Correspondence to: Dr Vishwa Jeet Amatya, Department of Pathology, Institute of Biomedical and Health Science, Hiroshima University, 1-2-3 Kasumi, Minami-ku, Hiroshima 734-8551, Japan
E-mail: amatya@hiroshima-u.ac.jp

Key words: CD9-shRNA, migration, CD9 immunohistochemistry, mesothelioma, survival

Introduction

CD9, a 24- to 27-kDa cell surface glycoprotein, is a member of the tetraspanin superfamily. It is expressed in numerous normal tissues and plays a critical role in various types of cell processes, such as cell adhesion, motility and various signaling pathways involving integrins. In malignancies, its expression usually suppresses tumor progression and metastasis by inhibition of tumor proliferation and survival (1,2). Although converse functions have also been reported in certain tumors, downregulation of CD9 correlates well with tumor progression or metastasis in bladder, breast, lung and colon cancers (2). An *in vivo* study using administration of the CD9 antibody to mice bearing human gastric cancer xenografts showed inhibition of tumor progression via anti-proliferative, pro-apoptotic and anti-angiogenetic effects (3), suggesting its potential for the molecular-targeted therapy of human malignancies. Moreover, we previously identified CD9, along with side population, CD24 and CD26 cells, as a cancer stem cell marker of mesothelioma, thus demonstrating its potential for cancer stem cell-targeted therapy in the future (4).

Malignant mesothelioma is an aggressive cancer with few patients surviving beyond 2 years following diagnosis. The median survival of patients without any treatment barely exceeds 1 year. A large population-based study reported 6-month, 1-year and 5-year overall survival rates of 55, 33 and 5% in mesothelioma (5). In Japanese patients, the median survival of mesothelioma has been reported to be 9-10 months from the date of diagnosis (6,7).

The clinical predictors for poor survival in patients with mesothelioma are reported to include sarcomatoid histology, older age, advanced IMIG stage, patients without palliative surgery or chemotherapy. Other biological prognostic factors such as serum and tumor EGFR expression (8,9), pleural effusion VEGF level (10), angiopoietin-1 expression (11), ER-β expression (12), methylation profile (6,13) and miRNA signatures (14) have also been reported. In this study, we identified CD9 as an independent predictor of survival, and loss of expression showed biological aggressive behavior in mesothelioma cells.

Materials and methods

Cell line. Mesothelioma cell lines, MSTO-211H [derived from biphasic mesothelioma (BM)] and TUM1 (4) were maintained in RPMI-1640 medium (Gibco-BRL; Invitrogen Life Technologies, Grand Island, NY) supplemented with 10% fetal calf serum (FCS), 100 U/ml penicillin and 100 mg/ml streptomycin. The cells were maintained as monolayers in 10-cm diameter cell culture dish at 37°C in a humidified atmosphere of 5% CO_2 in air.

shRNA lentiviral transfection. CD9-targeted shRNA lentiviral plasmid (Mission; Sigma-Aldrich, target sequence: ccgggctg ttcggatttaacttcatctcgagatgaagttaaatccgaacagctttttg) and non-targeting control plasmid (pLKO.1-puro) were transfected with ViraPower™ Lentiviral packaging mix to cell lines using Lipofectamine 2000 (Invitrogen Life Technologies). The cells were transfected with the shRNA-expressing lentivirus, and stable cell lines were generated by selection with puromycin. Knockdown of CD9 was confirmed by FACS analysis with the FITC mouse anti-human CD9 antibody (BD Pharmingen).

In vitro migration assay. Migration assay was performed using a 24-well Boyden chamber with a non-coated 8-mm pore size filter in the insert chamber (BD BioCoat). Cells (CD9 shRNA- and control shRNA-transfected MSTO-211H) ($5x10^4$) were suspended in 0.5 ml RPMI-1640 media containing 0.1% FCS and seeded into the insert chamber. Cells were allowed to migrate for 48 h into the bottom chamber containing 1 ml of RPMI-1640 media containing 10% FCS in a humidified incubator at 37°C in 5% CO_2. Migrated cells which had attached to the outside of the filter were visualized by staining with Diff-Quik (International Reagents Co.) and counted.

Patients and tissue specimens. One hundred and twelve cases of malignant pleural mesothelioma were retrieved from the archival pathology files of the Department of Pathology, Graduate School of Biomedical Sciences, Hiroshima University. Small biopsy specimens were not included in this study. The histological diagnosis of mesothelioma was previously carried out by three independent pathologists (V.J.A., Y.T., K.I.) based on WHO criteria (15) and were confirmed in all instances by clinical, histological and immunohistochemical findings. Epithelioid mesothelioma (EM) was further subdivided into two subtypes, i.e., 'differentiated' type (EM-D) and 'less-differentiated' type (EM-LD) based on the morphology of 'papillo-tubular structures' as an indicator of differentiation (16). Thus, EM-D were EMs showing a papillo-tubular pattern, micropapillary pattern and/or microcystic pattern and EM-LD were EMs showing solid nest, trabecular pattern, signet-ring cell-like appearance and/or single-cell infiltration pattern. The histological classification was carried out prior to this study. The clinical data of the patients were retrieved from the hospital records. This study was carried out in accordance with the Ethical Guidelines for Epidemiological Research enacted by the Japanese Government as tissue specimens were collected and carried out strictly to protect personal identity after approval by the Institutional Review Board at Hiroshima University.

Immunohistochemistry. Immunohistochemical stainings were performed on 3-μm paraffin sections using the monoclonal anti-CD9 antibody. Tissue sections were deparaffinized, hydrated and endogeneous peroxide was quenched using 0.3% hydrogen peroxidase for 30 min. Sections were incubated in a humidified chamber with mouse monoclonal anti-CD9 antibody (diluted 1:100, clone 72F6, NB110-41534; Novus Biologicals, Littleton, CO, USA) overnight at 4°C. The reaction was visualized using the Histofine Simple Stain kit (Nichirei Biosciences, Tokyo, Japan) with diaminobenzidine as a chromogen and nuclear counterstaining with Mayer's hematoxylin. A similar immunohistochemical procedure was carried out with the omission of the primary antibody as a negative control. Endothelial cells in and around the tumor tissue were considered as the internal positive control for validation of the immunohistochemistry. The membranous staining of CD9 was scored as 0, no staining; 1^+, 1-10%; 2^+, 10-50%; and 3^+, >50% of tumor cells immunostained in the tissue sections. Immunohistochemical scoring was carried out by two pathologists (V.J.A., Y.T.) independently without knowledge of the clinicopathologic or disease outcome variables. Multiple sections from different paraffin blocks were analyzed for CD9 expression to confirm negative CD9 expression.

Statistical analysis. Fisher's exact test and Pearson Chi-square test were used for association analyses of the clinicopathological parameters with CD9 expression. Univariate analysis and multivariate Cox proportional hazards regression analysis for overall survival were performed with the regressors: CD9 expression, age, gender, clinical IMIG staging, histological type, differentiation, therapeutic regimen, extrapleural pneumonectomy and chemotherapy status. The overall survival curves of patients with follow-up data were estimated using the Kaplan-Meier method. Multivariate Cox proportional hazard ratio (HR) was separately calculated for all mesotheliomas and EMs for patients with clinical data for all parameters including age, histology (in analyzing all cases)/differentiation (in analyzing EM alone), IMIG staging and therapeutic regimen. Statistical analysis of the migration assay was performed by the two-tailed t-test. All of the statistical analyses were carried out using JMP 9.0 software. P-value <0.05 was considered to indicate a statistically significant result.

Results

Effect of shRNA knockdown of CD9 on cell migration. Immunohistochemical analysis of CD9 expression in the patient mesothelioma samples indicated that CD9 expression was a favorable prognostic factor. Therefore, we investigated the effects of CD9 on the cell migration of mesothelioma cell lines using shRNA-mediated CD9 knockdown. Knockdown of CD9 in the MSTO-211H and TUM1 cell lines was confirmed by FACS analysis, and the migration of cells was analyzed using Boyden chamber assay (Fig. 1). CD9 shRNA-transfected and control shRNA-transfected MSTO-211H and TUM1 cells were allowed to migrate toward medium containing 10% FCS as a chemoattractant. CD9 shRNA-transfected MSTO-211H and TUM1 cells showed increased migration in comparison to the control shRNA-transfected cells (Fig. 1).

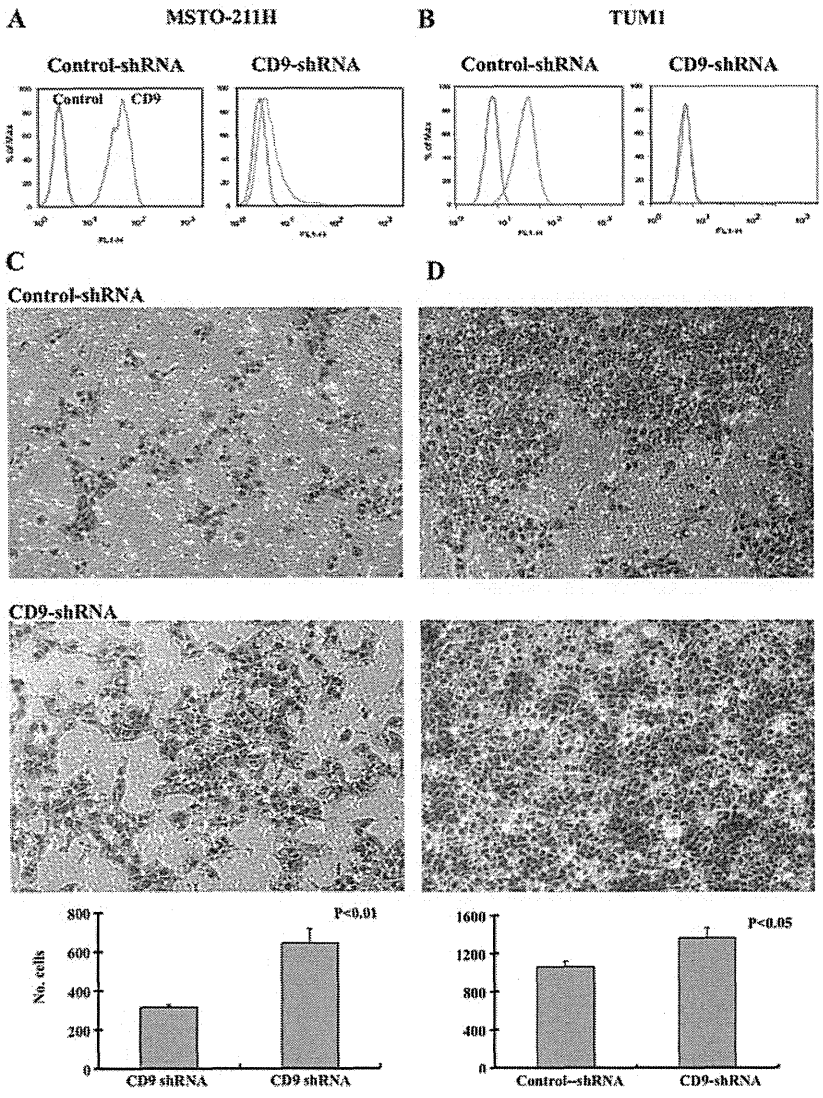

Figure 1. Flow cytometric analysis of CD9 expression in (A) MSTO-211H and (B) TUM1 cells transfected with control-shRNA and CD9-shRNA. Successful knockdown of CD9 was confirmed. Boyden chamber migration assay showed significantly increased cell migration of (C) MSTO-211H and (D) TUM1 cells transfected with CD9-shRNA (lower panels) in comparison to the control-shRNA (top panels).

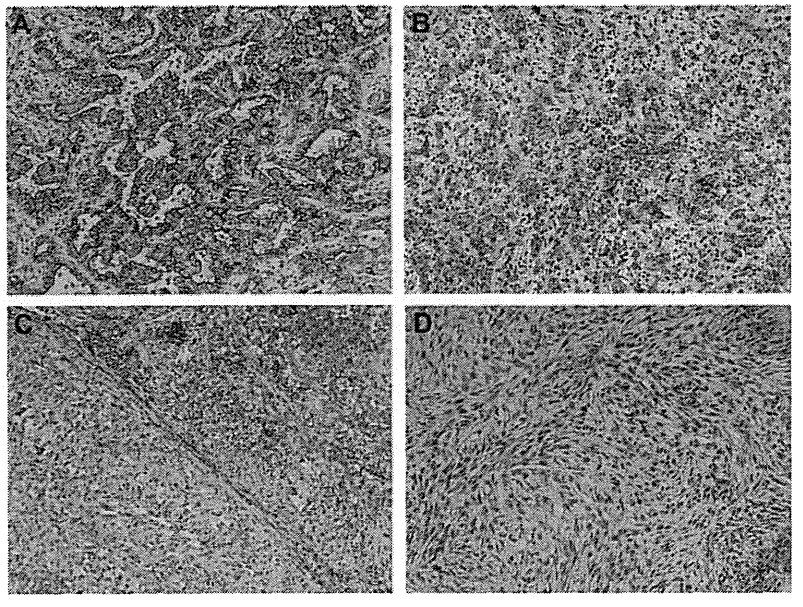

Figure 2. CD9 immunohistochemistry. (A) Epithelioid mesothelioma differentiated type showing diffuse CD9 expression. (B) Epithelioid mesothelioma less differentiated type showing decreased CD9 expression. (C) Biphasic mesothelioma showed CD9 expression in the epithelioid component while CD9 expression was not evident in the sarcomatoid component. (D) CD9 was not evident in the sarcomatoid component of sarcomatoid mesothelioma as well.

Table I. Immunohistochemical scoring of CD9 expression in malignant mesothelioma.

		CD9 immunohistochemical scoring			
Histology	Total cases	0	1	2	3
Epithelioid mesothelioma	71	9	21	25	16
Differentiated type	33	0	6	15	12
Less-differentiated type	38	9	15	10	4
Sarcomatoid mesothelioma	21	20	0	1	0
Biphasic mesothelioma	20	7	4	6	3

Table II. Clinicopathological characteristics of patients with mesothelioma and its correlation with CD9 expression.

	CD9 expression			
Clinicopathological parameters	Total cases	Positive	Negative	P-value[b]
Age (years)				
<60	35	30	5	0.0083
≥60	77	46	31	
Gender				
Male	103	68	35	0.2672
Female	9	8	1	
IMIG staging				
Stage I/II	65	48	17	0.1511
Stage III/IV	47	28	19	
Histology				
Epithelioid	71	62	9	<0.0001[c]
Sarcomatoid	21	1	20	
Biphasic	20	13	7	
Differentiation in epithelioid mesothelioma				
Differentiated	33	33	0	0.0027
Less-differentiated	38	29	9	
Therapeutic regimen				
BSC alone	30	18	12	0.0469[c]
Chemotherapy alone	42	25	17	
Extrapleural pneumonectomy[a]	40	33	7	
Extrapleural pneumonectomy (EPP)				
With EPP	40	33	7	0.0195
No EPP	72	43	29	
Chemotherapy				
With/without EPP and/or RT	74	50	24	1.0000
No chemotherapy	38	26	12	
Chemotherapy				
With pemetrexed	44	34	10	0.0434
Without pemetrexed	30	16	14	

IMIG, International Mesothelioma Interest Group; BSC, best supportive care; RT, radiotherapy. [a]This group consisted of patients receiving EPP alone or EPP with chemotherapy and/or radiotherapy. [b]Two-tailed Fisher's exact test. [c]Pearson's Chi-square test.

Clinicopathological characteristics of the malignant mesothelioma patients. This study consisted of 103 male patients and 9 female patients (M:F ratio 11:1), with a mean age of 65.8 years with standard deviation of 9.4 (range 42-88 years). Twenty-five cases were IMIG stage I, 40 cases were stage II, 25 cases were stage III and 21 cases were stage IV. Histologically, 71 cases were EMs (63.4%) 21 cases were sarcomatoid mesothelioma (SM) (18.75%) and 20 cases were BM (17.85%). Thirty-three

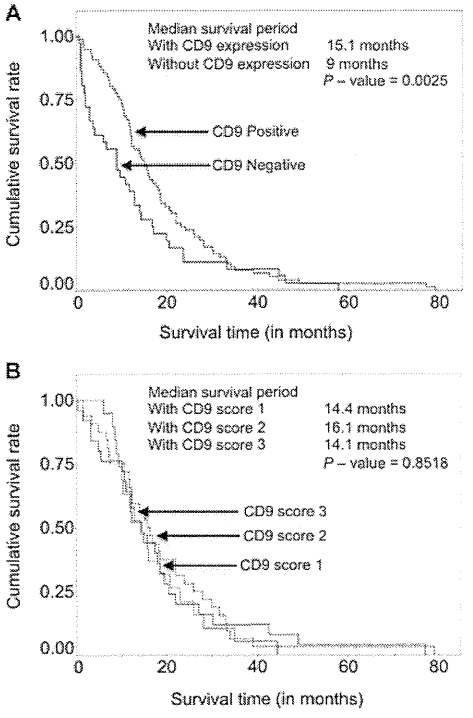

Figure 3. Kaplan-Meier curves showing overall survival of patients with mesothelioma in relation to CD9 expression status. (A) Patients with and without CD9 expression are represented by straight and dotted lines, respectively. (B) Patients with immunohistochemical score 1, 2 and 3 for CD9 expression showed no significance differences in overall survival.

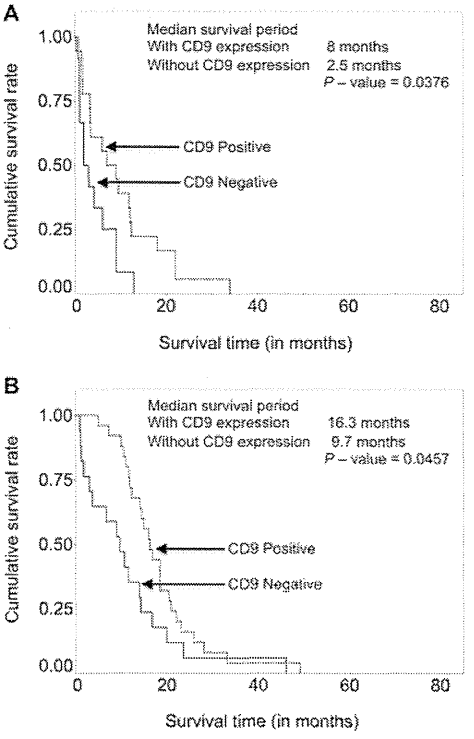

Figure 4. Kaplan-Meier survival curves showing overall survival of patients with mesothelioma with and without CD9 expression (A) receiving best supportive care and (B) receiving chemotherapy alone. Straight-line curve, without CD9 expression and dotted line curve, with CD9 expression.

cases of EM were differentiated type (EM-D) and 38 cases were less differentiated type (EM-LD).

Clinically, 30 patients received best supportive care alone, 42 patients were treated with chemotherapy alone and 40 cases underwent extrapleural pneumonectomy with or without chemotherapy and/or radiotherapy. Other surgical procedures were not included in this study as their numbers were limited for the analysis. The chemotherapy regimen consisted of various combinations: pemetrexed plus cisplatin regimen (39 cases), pemetrexed plus carboplatin (5 case), pemetrexed-containing regimen (44 cases) and chemotherapy regimens without pemetrexed (30 cases). The mean follow-up period was 16.5 months (from 10 days to 79 months) with 94 patients succumbing to the disease and 18 alive with disease at the time of the study.

CD9 expression in malignant mesothelioma. Positive immunoreactivity for CD9 was observed in the membrane and cytoplasm of the tumor cells in 76 of 112 malignant mesothelioma cases. Histologically, CD9 immunoreactivity was observed in 62 of 71 epithelioid mesotheliomas, 13 of 20 biphasic mesotheliomas and only 1 of 21 SMs. Among EMs, all cases of EM-D were CD9-positive and showed higher immunohistochemical score for CD9 expression compared to cases of EM-LD (Fig. 2) (Table I).

Association between CD9 expression and clinicopathological parameters. To determine the statistical significance of CD9 expression in malignant mesothelioma, all cases were divided into two groups based on their CD9 expression: a CD9-positive (n=76, 67.9%) and a CD9-negative (n=36, 32.1%) group. The association between CD9 expression and various clinicopathological parameters is listed in Table II. Mesothelioma patients with a younger age (P=0.0083), epithelioid histology (P<0.0001), differentiated type EMs (P=0.0027), who did not receive best supportive care (P=0.0469), who underwent EPP and chemotherapy (P=0.0195) and who received chemotherapy with inclusion of pemetrexed (P=0.0434) showed statistically significantly a high frequency of positive CD9 expression.

Association between CD9 expression and patient prognosis. The median survival period for the CD9-positive group was 15.1 months and that for the CD9-negative group was 9 months. The difference between the two groups was statistically significant (Wilcoxon; P=0.0025) (Fig. 3A). However, when CD9 expression was stratified according to immunohistochemical scores, no significant association was noted between CD9 expression score and patient survival (Fig. 3B). The CD9-positive group showed higher 1- and 2-year survival rates (63.2 and 25.0%) compared to the CD9-negative group (38.9 and 11.1%) (Table III).

Among the patients receiving best supportive care, patients with CD9 expression had higher survival (mean survival time 8 months) compared to those without CD9 expression (mean survival time, 2.5 months) (P=0.0376). A similar result was found among the patients treated with chemotherapy alone with a mean survival time of 16.2 months for patients with CD9 expression and 9.7 months for patients without CD9 expression (P=0.0037) (Fig. 4).

Other clinicopathological parameters that correlated significantly with overall survival according to univariate

Table III. Univariate analysis of overall survival in patients with malignant mesothelioma.

Clinicopathological parameters	Survival in months		1-year survival	2-year survival	P-value
	Median	Mean			
Age (years)					
<60	22.0	25.4	77.1%	42.9%	0.0003
≥60	11.6	12.6	45.5%	10.4%	
Gender					
Male	12.2	15.3	53.4%	18.5%	0.0789
Female	18.0	30.7	77.8%	44.4%	
IMIG staging					
Stage I/II	16.3	20.4	63.5%	30.2%	0.0001
Stage III/IV	9.0	9.9	42.4%	3.1%	
Histology					
Epithelioid	15.7	19.5	63.4%	29.6%	<0.0001
Sarcomatoid	3.8	6.1	14.3%	0%	
Biphasic	13.9	17.0	70.0%	10.0%	
Differentiation in epithelioid mesothelioma					
Differentiated	18.6	22.5	72.7%	36.4%	0.0301
Less differentiated	14.0	17.0	55.3%	23.7%	
Therapeutic regimen					
BSC	5.1	7.7	23.3%	3.3%	<0.0001
Chemotherapy alone	14.2	15.3	57.1%	11.9%	
Extrapleural pneumonectomy	18.9	24.5	77.5%	42.5%	
Extrapleural pneumonectomy					
With EPP	18.9	24.5	77.5%	42.5%	<0.0001
Without EPP	11.0	12.1	43.1%	8.3%	
Chemotherapy					
With/without EPP and/or RT	16.5	19.7	70.3%	27.0%	<0.0001
No chemotherapy	6.4	11.0	26.3%	7.9%	
Chemotherapy					
With pemetrexed	18.4	21.2	81.8%	29.6%	0.0715
Without pemetrexed	13.4	17.4	53.3%	23.3%	
CD9 expression					
Positive	15.1	18.4	63.2%	25.0%	0.0025
Negative	9	12.6	38.9%	11.1%	

IMIG, International Mesothelioma Interest Group; BSC, best supportive care; EPP, extrapleural pneumonectomy; RT, radiotherapy.

analysis (Table III) included age (P=0.0003), IMIG staging (P=0.0001), histology (P<0.0001), differentiation (P=0.0301), therapeutic regimen (P=<0.0001), extrapleural pneumonectomy (P<0.0001) and chemotherapy (P<0.0001). Chemotherapy with inclusion of pemetrexed showed a tendency for better survival, but did not achieve statistical significance (P=0.0715). Multivariate analysis using the Cox proportional hazards model of mesothelioma patients showed loss of CD9 expression as an independent predictor of overall survival in patients with malignant mesothelioma with an HR 1.99 (P=0.0261) in addition to age, IMIG staging, histology and therapeutic regimen (Table IV). As the CD9 expression in EMs showed a significant difference in the differentiation type, we also analyzed multivariate analysis using Cox proportional hazards model of 71 EMs. CD9 expression was again an independent predictor of overall survival with an HR of 2.60 (P=0.0376) along with other factors; age (P=0.0023) therapeutic regimens, chemotherapy (P=0.0113) and extrapleural pneumonectomy (P=0.0014), but not IMIG staging (P=0.1336) and differentiation (P=0.1337) (Table V).

Discussion

Disruption of cell adhesion and alteration in cell motility play an important role in cancer cell invasion and metastasis. The tetraspanin superfamily proteins (TM4SF) mainly CD9, CD63, CD82, CD151 and CD81 have been implicated in cell migration, proliferation and tumor cell metastasis (17,18). CD9 is to date the best characterized member of the TM4SF proteins and is involved in cell growth, adhesion and motility. Moreover, CD9

Table IV. Multivariate analysis of overall survival in malignant mesothelioma (Cox proportional hazards model).

Prognostic factors	Hazard ratio	95% confidence interval		P-value
		Lower	Upper	
CD9 expression	1.99	1.08	3.82	0.0261
Age, 60 years or more	2.10	1.24	3.66	0.0053
IMIG stage III/IV	2.04	1.23	3.37	0.0059
Histology against epithelioid mesothelioma				
Biphasic mesothelioma	2.13	1.15	3.87	0.0171
Sarcomatoid mesothelioma	6.65	2.91	15.22	<0.0001
Therapeutic regimen against BSC				
Chemotherapy alone	0.37	0.21	0.67	0.0011
Extrapleural pneumonectomy	0.26	0.14	0.50	<0.0001

BSC, best supportive care; IMIG, International Mesothelioma Interest Group.

Table V. Multivariate analysis of overall survival in epithelioid mesothelioma (Cox proportional hazards model).

Prognostic factors	Hazard ratio	95% confidence interval		P-value
		Lower	Upper	
CD9 expression	2.60	1.05	7.37	0.0376
Age, 60 years or more	2.62	1.40	5.12	0.0023
IMIG stage III/IV	1.64	0.85	3.11	0.1336
Less-differentiated type	1.54	0.87	2.71	0.1337
Therapeutic regimen against BSC				
Chemotherapy alone	0.37	0.18	0.79	0.0113
Extrapleural pneumonectomy	0.27	0.12	0.59	0.0014

BSC, best supportive care; IMIG, International Mesothelioma Interest Group.

has been recently reported as a prognostic factor in adenocarcinoma of the lung (19), colon (20), breast (21), pancreas (22), prostate (23) and SCC of the esophagus (24) and oral cavity (25). We found increased cell migration in CD9-knockdown mesothelioma cell lines. In this migration assay experiment using MSTO-211H cells, we found a decrease in CD9 expression after CD9-shRNA transfection which led to increased cell migration compared to control-shRNA-transfected cells.

These data suggest the importance of CD9 in determining the aggressive behavior of malignant mesothelioma. Recently, Nakamoto *et al* (3) investigated the antitumor effect of the anti-CD9 monoclonal antibody (ALB6) in human gastric cancer cell xenografts. They found a profound effect on tumor progression by anti-proliferative, pro-apoptotic and anti-angiogenetic effects. Moreover, we previously identified CD9 along with side population CD24 and CD26 cells to be markers of cancer stem cells in mesothelioma. We also demonstrated that CD9-positive cell lines had a clear tendency to generate larger tumors in mice (4). Thus, CD9 may be a potential candidate as a molecular target in the treatment of mesothelioma.

Loss of CD9 expression correlates with poor prognosis in bladder carcinoma (26) and esophageal squamous cell carcinoma (24), small and non-small cell lung cancers (27,28) and prostatic carcinoma (23). This study is the first to analyze CD9 expression in human mesothelioma tissue and to correlate its expression with survival with other clinicopathological parameters. CD9 expression was noted more frequently in younger patients, IMIG stage I-II and epithelioid histology compared to older patients, IMIG stage III-IV and sarcomatoid histology.

The present study found that the loss of CD9 expression in mesothelioma is related to a shorter overall survival (medial survival 9 months, 1-year survival 38.9% and 2-year survival 11.1%) compared to patients with CD9 expression (median survival 15.1 months, 1-year survival, 63.2% and 2-year survival 25%). When CD9 expression in mesothelioma was stratified according to score (1-3) did not show a statistically significant association with overall survival rates (Fig. 3B), suggesting that the complete loss of CD9 expression has more significance than the extent of CD9 expression. Age, IMIG staging, histology, differentiation of epithelioid mesothelioma, therapeutic regimen, status of extrapleural pneumonectomy and status of chemotherapy all had a statistically significant association with overall survival. Patients with CD9 expression had higher survival compared to those without CD9 expression

in patients receiving best supportive care or patients treated with chemotherapy. This suggests the importance of CD9 expression as an indicator for patients receiving chemotherapy in mesothelioma patients.

The multivariate analysis showed CD9 expression is an independent predictor of survival of mesothelioma patients with an HR of 1.99 (P=0.0261) as well as older age (HR, 2.10), IMIG stage III/IV (HR, 2.04), sarcomatoid histology (HR, 6.65), patients treated with chemotherapy alone (HR, 0.37) and patients treated with extrapleural pneumonectomy (HR, 0.26) (Table IV). As CD9 expression was observed in only one case of sarcomatoid mesothelioma and sarcomatoid histology was itself a strong independent predictor of survival of mesothelioma patients, multivariate analysis excluding sarcomatoid mesothelioma is necessary to evaluate the importance of CD9 expression as an independent predictor of mesothelioma survival. Hence, we performed multivariate analysis of patients with epithelioid mesothelioma alone and we again found that CD9 expression was a predictor of survival of mesothelioma patients with an HR of 2.60 (P=0.0376) (Table V), suggesting the independent prognostic value of CD9 expression in mesothelioma.

In the present study, sarcomatoid mesothelioma did not show CD9 expression. It may thus be hypothesized that the loss of CD9 expression in epithelioid mesothelioma leads to loss of epithelioid differentiation and ultimately transition into sarcomatoid mesothelioma. This is supported, in part, by the fact that histologically less-differentiated epithelioid mesotheliomas showed lower CD9 expression. In contrast, loss of differentiation or epithelial-mesenchymal transition by other molecular pathways leading to loss of CD9 expression may also be postulated. The biological significance of loss of CD9 expression in sarcomatoid mesothelioma requires further investigation.

In conclusion, CD9 expression is a favorable prognostic marker in patients with mesothelioma. Our *in vitro* study demonstrated increased cell migration after CD9 knockdown, suggesting loss of CD9 as a predictor of more aggressive behavior. CD9 expression may be also an indicator of epithelial-mesenchymal transition from epithelioid mesothelioma to sarcomatoid mesothelioma.

Acknowledgements

The authors thank Yuka Fukushima for her excellent technical assistance and Keiko Honda and Naomi Fukuhara for their administrative assistance. This research was supported by the Program for the Promotion of Fundamental Studies in Health Sciences of the National Institute of Biomedical Innovation.

References

1. Tarrant JM, Robb L, van Spriel AB and Wright MD: Tetraspanins: molecular organisers of the leukocyte surface. Trends Immunol 24: 610-617, 2003.
2. Zoller M: Tetraspanins: push and pull in suppressing and promoting metastasis. Nat Rev Cancer 9: 40-55, 2009.
3. Nakamoto T, Murayama Y, Oritani K, *et al*: A novel therapeutic strategy with anti-CD9 antibody in gastric cancers. J Gastroenterol 44: 889-896, 2009.
4. Ghani FI, Yamazaki H, Iwata S, *et al*: Identification of cancer stem cell markers in human malignant mesothelioma cells. Biochem Biophys Res Commun 404: 735-742, 2011.
5. Milano MT and Zhang H: Malignant pleural mesothelioma: a population-based study of survival. J Thorac Oncol 5: 1841-1848, 2010.
6. Kobayashi N, Toyooka S, Yanai H, *et al*: Frequent p16 inactivation by homozygous deletion or methylation is associated with a poor prognosis in Japanese patients with pleural mesothelioma. Lung Cancer 62: 120-125, 2008.
7. Nojiri S, Gemba K, Aoe K, *et al*: Survival and prognostic factors in malignant pleural mesothelioma: a retrospective study of 314 patients in the west part of Japan. Jpn J Clin Oncol 41: 32-39, 2011.
8. Gaafar R, Bahnassy A, Abdelsalam I, *et al*: Tissue and serum EGFR as prognostic factors in malignant pleural mesothelioma. Lung Cancer 70: 43-50, 2010.
9. Rena O, Boldorini LR, Gaudino E and Casadio C: Epidermal growth factor receptor overexpression in malignant pleural mesothelioma: prognostic correlations. J Surg Oncol 104: 701-705, 2011.
10. Hirayama N, Tabata C, Tabata R, *et al*: Pleural effusion VEGF levels as a prognostic factor of malignant pleural mesothelioma. Respir Med 105: 137-142, 2011.
11. Tabata C, Hirayama N, Tabata R, *et al*: A novel clinical role for angiopoietin-1 in malignant pleural mesothelioma. Eur Respir J 36: 1099-1105, 2010.
12. Pinton G, Brunelli E, Murer B, *et al*: Estrogen receptor-beta affects the prognosis of human malignant mesothelioma. Cancer Res 69: 4598-4604, 2009.
13. Fischer JR, Ohnmacht U, Rieger N, *et al*: Promoter methylation of RASSF1A, RARbeta and DAPK predict poor prognosis of patients with malignant mesothelioma. Lung Cancer 54: 109-116, 2006.
14. Pass HI, Goparaju C, Ivanov S, *et al*: hsa-miR-29c* is linked to the prognosis of malignant pleural mesothelioma. Cancer Res 70: 1916-1924, 2010.
15. Travis W, Brambilla E, Müller-Hermelink H and Harris C (eds): World Health Organization Classification of Tumours: Pathology & Genetics. Tumours of the Lung, Pleura, Thymus and Heart. IARC Press, Lyon, 2004.
16. Amatya VJ, Takeshima Y, Kushitani K, Yamada T, Morimoto C and Inai K: Overexpression of CD26/DPPIV in mesothelioma tissue and mesothelioma. Oncol Rep 26: 1369-1375, 2011.
17. Ikeyama S, Koyama M, Yamaoko M, Sasada R and Miyake M: Suppression of cell motility and metastasis by transfection with human motility-related protein (MRP-1/CD9) DNA. J Exp Med 177: 1231-1237, 1993.
18. Miyake M, Koyama M, Seno M and Ikeyama S: Identification of the motility-related protein (MRP-1), recognized by monoclonal antibody M31-15, which inhibits cell motility. J Exp Med 174: 1347-1354, 1991.
19. Higashiyama M, Doi O, Kodama K, *et al*: Immunohistochemically detected expression of motility-related protein-1 (MRP-1/CD9) in lung adenocarcinoma and its relation to prognosis. Int J Cancer 74: 205-211, 1997.
20. Mori M, Mimori K, Shiraishi T, *et al*: Motility related protein 1 (MRP1/CD9) expression in colon cancer. Clin Cancer Res 4: 1507-1510, 1998.
21. Jamil F, Peston D and Shousha S: CD9 immunohistochemical staining of breast carcinoma: unlikely to provide useful prognostic information for routine use. Histopathology 39: 572-577, 2001.
22. Sho M, Adachi M, Taki T, *et al*: Transmembrane 4 superfamily as a prognostic factor in pancreatic cancer. Int J Cancer 79: 509-516, 1998.
23. Wang JC, Begin LR, Berube NG, *et al*: Down-regulation of CD9 expression during prostate carcinoma progression is associated with CD9 mRNA modifications. Clin Cancer Res 13: 2354-2361, 2007.
24. Okochi H, Mine T, Nashiro K, Suzuki J, Fujita T and Furue M: Expression of tetraspans transmembrane family in the epithelium of the gastrointestinal tract. J Clin Gastroenterol 29: 63-67, 1999.
25. Buim ME, Lourenco SV, Carvalho KC, *et al*: Downregulation of CD9 protein expression is associated with aggressive behavior of oral squamous cell carcinoma. Oral Oncol 46: 166-171, 2010.
26. Mhawech P, Herrmann F, Coassin M, Guillou L and Iselin CE: Motility-related protein 1 (MRP-1/CD9) expression in urothelial bladder carcinoma and its relation to tumor recurrence and progression. Cancer 98: 1649-1657, 2003.
27. Higashiyama M, Taki T, Ieki Y, *et al*: Reduced motility related protein-1 (MRP-1/CD9) gene expression as a factor of poor prognosis in non-small cell lung cancer. Cancer Res 55: 6040-6044, 1995.
28. Kohmo S, Kijima T, Otani Y, *et al*: Cell surface tetraspanin CD9 mediates chemoresistance in small cell lung cancer. Cancer Res 70: 8025-8035, 2010.

PLOS ONE

Cardiomyocyte-Specific Overexpression of HEXIM1 Prevents Right Ventricular Hypertrophy in Hypoxia-Induced Pulmonary Hypertension in Mice

Noritada Yoshikawa[1☯], Noriaki Shimizu[1☯], Takako Maruyama[1], Motoaki Sano[2], Tomohiro Matsuhashi[2], Keiichi Fukuda[2], Masaharu Kataoka[2,3], Toru Satoh[3], Hidenori Ojima[4], Takashi Sawai[5], Chikao Morimoto[6], Akiko Kuribara[1], Osamu Hosono[1], Hirotoshi Tanaka[1]*

1 Department of Rheumatology and Allergy, IMSUT Hospital, Institute of Medical Science, The University of Tokyo, Tokyo, Japan, **2** Department of Cardiology, Keio University School of Medicine, Tokyo, Japan, **3** Department of Cardiology, Kyorin University School of Medicine, Mitaka, Tokyo, Japan, **4** Pathology Division, National Cancer Center Research Institute, Tokyo, Japan, **5** Department of Pathology, Iwate Medical University School of Medicine, Shiwa-gun, Iwate, Japan, **6** Department of Therapy Development and Innovation for Immune Disorders, Juntendo University, Tokyo, Japan, Cancers, Graduate School of Medicine, Juntendo University, Tokyo, Japan

Abstract

Right ventricular hypertrophy (RVH) and right ventricular (RV) contractile dysfunction are major determinants of prognosis in pulmonary arterial hypertension (PAH) and PAH remains a severe disease. Recently, direct interruption of left ventricular hypertrophy has been suggested to decrease the risk of left-sided heart failure. Hexamethylene bis-acetamide inducible protein 1 (HEXIM1) is a negative regulator of positive transcription elongation factor b (P-TEFb), which activates RNA polymerase II (RNAPII)-dependent transcription and whose activation is strongly associated with left ventricular hypertrophy. We hypothesized that during the progression of PAH, increased P-TEFb activity might also play a role in RVH, and that HEXIM1 might have a preventive role against such process. We revealed that, in the mouse heart, HEXIM1 is highly expressed in the early postnatal period and its expression is gradually decreased, and that prostaglandin I_2, a therapeutic drug for PAH, increases HEXIM1 levels in cardiomyocytes. These results suggest that HEXIM1 might possess negative effect on cardiomyocyte growth and take part in cardiomyocyte regulation in RV. Using adenovirus-mediated gene delivery to cultured rat cardiomyocytes, we revealed that overexpression of HEXIM1 prevents endothelin-1-induced phosphorylation of RNAPII, cardiomyocyte hypertrophy, and mRNA expression of hypertrophic genes, whereas a HEXIM1 mutant lacking central basic region, which diminishes P-TEFb-suppressing activity, could not. Moreover, we created cardiomyocyte-specific HEXIM1 transgenic mice and revealed that HEXIM1 ameliorates RVH and prevents RV dilatation in hypoxia-induced PAH model. Taken together, these findings indicate that cardiomyocyte-specific overexpression of HEXIM1 inhibits progression to RVH under chronic hypoxia, most possibly via inhibition of P-TEFb-mediated enlargement of cardiomyocytes. We conclude that P-TEFb/HEXIM1-dependent transcriptional regulation may play a pathophysiological role in RVH and be a novel therapeutic target for mitigating RVH in PAH.

Citation: Yoshikawa N, Shimizu N, Maruyama T, Sano M, Matsuhashi T, et al. (2012) Cardiomyocyte-Specific Overexpression of HEXIM1 Prevents Right Ventricular Hypertrophy in Hypoxia-Induced Pulmonary Hypertension in Mice. PLoS ONE 7(12): e52522. doi:10.1371/journal.pone.0052522

Editor: Masataka Kuwana, Keio University School of Medicine, Japan

Received October 3, 2012; **Accepted** November 14, 2012; **Published** December 31, 2012

Funding: This work was supported by Grants-in-Aid for Scientific Research (B) to HT (24390236), for Young Scientists (B) to NY (22790693) and NS (23791050), and for Encouragement of Scientists to TM (24930026), grants from the Ministry of Health, Labour, and Welfare to HT, grants from Takeda Science Foundation and Suzuken Memorial Foundation to NS, and grant from Actelion Academia Prize (Actelion Pharmaceuticals) to NY. The funders had no role in study design, data collection and analysis, decision to publish, or preparation of the manuscript.

Competing Interests: With respect to funding from Actelion Pharmaceuticals, the authors do not have any other relevant declarations such as employment, consultancy, patents, products in development or marketed products, and their funding does not alter the authors' adherence to all the PLOS ONE policies on sharing data and materials.

* E-mail: hirotnk@ims.u-tokyo.ac.jp

☯ These authors contributed equally to this work.

Introduction

Pulmonary arterial hypertension (PAH) occurs in a variety of clinical situations and is a syndrome in which pulmonary arterial obstruction increases pulmonary vascular resistance, which leads to right ventricular hypertrophy (RVH) and right ventricular (RV) failure. PAH is associated with a broad spectrum of histological abnormalities including intimal lesions, medial hypertrophy, and adventitial thickening of precapillary pulmonary arteries and RVH [1]. Although recent advance in treatment of PAH, including prostacyclin analogs (e.g., prostaglandin I_2, PGI_2), endothelin-1 (ET-1) receptor blockades, and phosphodiesterase type 5 (PDE-5) inhibitors, improved prognosis of PAH patients, RVH and contractile dysfunction of RV are major determinants of prognosis in PAH and the mortality of PAH patients still remains high [1–3]. Surprisingly, little is known about the specific mechanisms underlying RVH and dysfunction of RV in the setting of PAH. Although the obvious approach to reducing RVH and RV failure is to treat the underlying pulmonary artery disease, recent evidence suggests that the RV can be targeted therapeutically in PAH [4,5]. Indeed, direct interruption of cardiac remodeling, i.e., cardiac hypertrophy, has been suggested to be

beneficial to decrease the risk of heart failure [6,7]. In this line, the PDE-5 inhibitor added to conventional treatment reduces RV mass and improves cardiac function and exercise capacity in patients with PAH, suggesting that the drugs which have combined effects on both RV and pulmonary artery may be more advantageous than drugs that affect only the pulmonary artery [8–10].

An RNA-binding protein hexamethylene bis-acetamide inducible protein 1 (HEXIM1) was originally identified as a nuclear protein, expression of which was induced when human vascular smooth muscle cells were treated with hexamethylene bisacetamide (HMBA), an inhibitor of cell proliferation [11]. HEXIM1 is thought to be composed of several functional domains: a variable N-terminal self-inhibitory domain, a central basic region that acts as nuclear localization signal (NLS) and interacts with the nuclear transport machinery as well as binds directly to 7SK small nuclear RNA (snRNA), an adjacent region of which might be involved in inhibition of positive transcription elongation factor-b (P-TEFb), and the C-terminus, the Cyclin T-binding domain leads to dimerization of HEXIM1 molecules. P-TEFb is composed of cyclin-dependent kinase 9 (Cdk9) and cyclin T1 and phosphorylates the carboxyl-terminal domain (CTD) of RNA polymerase II (RNAPII), and upon phosphorylation elongates nascent transcripts to form full-length messenger RNAs. HEXIM1 forms a protein–RNA complex, termed the 7SK small nuclear ribonucleoprotein complex (snRNP) composed of 7SK snRNA and P-TEFb, and inhibits the kinase activity of Cdk9, leading to the suppression of RNAPII-dependent transcriptional elongation [12,13]. On the other hand, HEXIM1 modulates gene expression in a unique fashion. For example, HEXIM1 has been shown to directly bind and variably modulate the activities of transcription factors including estrogen receptor alpha, glucocorticoid receptor, CCAAT/enhancer-binding protein alpha, and nuclear factor-kappa B [14–19].

It has been reported that Cdk9 activity was demonstrated to be necessary for hypertrophy in cardiomyocytes in vitro and that heart-specific activation of Cdk9 was found to provoke left ventricular hypertrophy (LVH) in mice, suggesting that the increase in P-TEFb function is associated with LVH [20]. In this line, deletion of the cardiac lineage protein-1 (CLP-1) gene, which is a mouse homolog of human HEXIM1, in mice results in embryonic lethality. An analysis of CLP-$1^{-/-}$ fetal hearts indicated a hypertrophic phenotype, indicating that dysregulation of the 7SK snRNP by the genetic ablation of CLP-1/HEXIM1 can also contribute to LVH [21]. The dissociation of CLP-1/HEXIM1 from P-TEFb was shown to be responsive to hypertrophic stimuli in cardiomyocytes [22]. Siddiqui and colleagues generated two different bigenic mice (alphaMHC–cyclin T1/CLP-$1^{+/-}$ and alphaMHC–angiotensin II/CLP-$1^{+/-}$) by crossing alpha-MHC promoter-driven cyclin T1 or angiotensin II expressing transgenic mice with CLP-1 heterozygote, respectively. These bigenic mice exhibit enhanced susceptibility to LVH that is accompanied with an increase in Cdk9 activity via an increase in Ser2 phosphorylation of CTD or with activation of angiotensin II-TGF-beta1-CLP-1-Smad3 signaling axis and natriuretic peptide expression, respectively [23,24]. HEXIM1 has also been known to have antiangiogenic effect by preventing estrogen-induced vascular endothelial growth factor (VEGF) transcription through inhibition of estrogen receptor-alpha recruitment to the VEGF promoter in MCF-7 breast cancer cells [25]. On the other hand, an analysis of the mice carrying an insertional mutation in the HEXIM1 gene that disrupted its C-terminal region indicated that HEXIM1 plays critical roles in coronary vessel development and myocardial growth and that VEGF is a direct transcriptional target of HEXIM1 [18]. Moreover, there was a significant increase in the levels of hypoxia-inducible factor 1 alpha (HIF-1alpha) protein in CLP-$1^{+/-}$ hearts subjected to ischemic stress as compared to CLP-$1^{+/+}$ hearts treated identically, suggesting that HEXIM1 could affect HIF-1-dependent transcription [26]. Despite these numerous analyses, the role of HEXIM1 in RV pathophysiology has not yet been studied.

In this report, we revealed that HEXIM1 is highly expressed in the early postnatal period and its expression is gradually decreased in the mouse heart. Adenovirus-mediated HEXIM1 gene delivery to ET-1-stimulated cardiomyocytes caused inhibition of P-TEFb activity and cardiomyocyte enlargement. Moreover, using a cardiomyocyte-specific transgenic mouse expressing exogenous HEXIM1 and chronic hypoxia-driven PAH model, we indicated that cardiomyocyte HEXIM1 may inhibit progression to RVH in PAH.

Materials and Methods

Ethics Statement

Human autopsy hearts were obtained with written informed consent from the families and analyzed at Iwate Medical University under the approval from the Ethics Committees of the Iwate Medical University. All animal experimental procedures and protocols were approved by the Animal Experiment Committee of Institute of Medical Science, The University of Tokyo, and the Animal Care and Use Committee of Keio University, and conducted according to the institutional ethical guidelines for animal experiments.

Samples of Human Biological Material

INSTA-Blot™ Human Tissues IMB-103 (IMGENEX, San Diego, CA) is a ready-to-use polyvinyl difluoride (PVDF) membrane, which contains denatured proteins from human lysates loaded at 20 micrograms per lane on a 4–20% Tris-Glycine mini gel, resolved by SDS- polyacrylamide gel electrophoresis, and transferred. Formalin-fixed human autopsy hearts were analyzed by immunohistochemistry according to a standard protocol as described previously [27].

Animals

C57BL/6J mice and Wistar rats were obtained from CLEA Japan (Tokyo, Japan). PGI_2 synthetase–null mice ($PGIS^{-/-}$) were kindly provided from Dr. Tadashi Tanabe (Department of Pharmacology, National Cardiovascular Center Research Institute, Osaka, Japan) [28]. The heterozygous mice expressing Cre recombinase driven by the alpha-MHC promoter (alphaMHC-Cre) were kindly provided from Dr. Kinya Otsu (Department of Internal Medicine and Therapeutics, Osaka University Graduate School of Medicine, Osaka, Japan) [29].

Reagents and Antibodies

ET-1 (E7764), PGI_2 (P6188), Sildenafil (PZ0003), BQ123 (B150), HMBA (224235), and anti-alpha-actinin (A7811) and -FLAG (M2) antibodies were purchased from Sigma-Aldrich (St. Louis, MO). Anti-human HEXIM1 antibodies, which can cross-react with rodent HEXIM1, were generated as previously described [19]. Mouse HEXIM1-specific antiserum was generated by immunizing a rabbit with peptide SGSRPGQEGEGGLKH corresponding to amino acids 55–69 of mouse HEXIM1. Anti-RNAPII antibodies (8WG16, H5, and H14 for recognizing C-terminal heptapeptide repeat, phosphoserine 2, and phosphoserine 5, respectively) were purchased from Covance (Princeton, NJ). Anti-Cdk9 (C-20), -CycT1 (H-245), -actin (C-2), -S6K (C-18), and

-extracellular signal regulated kinase 2 (ERK2, C-14) antibodies were obtained from Santa Cruz Biotechnologies (Santa Cruz, CA). Anti-phospho S6K (Thr389, 105D2), -phospho-p38 mitogen-activated protein kinase (p38 MAPK, Thr180/Tyr182, 3D7), -p38 MAPK (#9212), -phospho-c-Jun N-terminal kinase (JNK, Thr183/Tyr185, 81E11), -JNK (#9252), and -phospho-ERK1/2 (Thr202/Tyr204, #9101) antibodies were purchased from Cell Signaling Technology (Beverly, MA). The branched-chain amino acids (BCAA) cocktail (L-leucine:L-isoleucine:L-valine =2:1:1.2) was prepared as described previously [30]. Other reagents were obtained from Nacalai Tesque (Kyoto, Japan) unless otherwise specified.

Cell Culture

Primary cultures of neonatal rat cardiomyocytes (NRCM) and cardiac fibroblasts were prepared as described previously [31]. In brief, the ventricles of 1-day-old neonatal Wistar rats were dissociated in 0.03% trypsin, 0.03% collagenase, and 20 μg/mL of DNase I. The cardiomyocytes and fibroblasts were separately prepared on the basis of their differential adhesiveness. Attached cells were subcultured two times to deplete residual cardiomyocytes, and the third passage cells were used as cardiac fibroblasts. NRCM were separated from cardiac fibroblasts and seeded at a density of 1×10^5 cells/cm^2 on gelatin-coated dishes. Both cells were grown in medium 199/DMEM (Invitrogen, Carlsbad, CA) supplemented with 10% fetal calf serum and antibiotics in a humidified atmosphere at 37°C with 5% CO_2. The culture media was replaced to phenol red and serum-free medium Opti-MEM I (Invitrogen) and further cultured for 24 hr before various treatments or adenovirus infection of the cells unless otherwise specified.

Recombinant Adenoviruses

Recombinant adenoviruses encoding FLAG- and 6×histidine (FLAG-His)-tagged human HEXIM1 (AdCALNL/FHhHEXIM1) and its mutant (AdCALNL/FHhHEXIM1dBR+SV), in which the central NLS of HEXIM1 was replaced to the simian 40 virus large T-antigen NLS, preceded by a floxed stuffer sequence were generated by using Adenovirus Cre/loxP-regulated Expression Vector Set (TaKaRa, Otsu, Japan) as manufacturer's instructions and previously described [15,17]. Recombinant adenoviruses encoding double-stranded hairpin RNAs for siRNA against HEXIM1, AdsiHEXIM1, or control siRNA, Adsictrl, were described previously [15,17]. Recombinant adenoviruses encoding Cre-recombinase (AxCANCre) and beta-galactosidase (AxCALNLZ, used as irrelevant adenovirus) were purchased from Takara. These adenoviruses prepared from 293 cells were purified with Virakit AdenoMini-24 (Virapur, San Diego, CA) and titrated using Adeno-X Rapid Titer Kit (TaKaRa).

Recombinant Proteins

Oligo DNA 5′-CATGGACTACAAAGACGATGACGACAAGGG-3′ and 5′-CATGCCCTTGTCGTCATCGTCTTTGTAGTC-3′ were annealed and inserted into NcoI site of pET14b (Merck KGaA, Darmstadt, Germany) to generate a bacterial expression plasmid for FLAG-His-tagged recombinant protein (named pFLET). Human and mouse HEXIM1 cDNA were cloned into NdeI-XhoI sites of pFLET to generate pFLET-hHEXIM1 and pFLET-mHEXIM1, respectively. Plasmids constructed above were verified by DNA sequencing. FLAG-His-tagged human and mouse HEXIM1 recombinant proteins were expressed in E. coli strain Rosetta 2 (DE3) pLysS (Stratagene, La Jolla, CA) transformed by pFLET-hHEXIM1 and pFLET-mHEXIM1, respectively. E. coli were cultured at 30°C in MagicMedia E. coli Expression Medium (Invitrogen) containing 100 μg/ml ampicillin for 12 hr, lysed in E. coli lysis buffer (25 mmol/L Tris-HCl, pH 7.9, 500 mmol/L NaCl, 0.1% Nonidet-P40, 0.5 mmol/L phenylmethylsulfonyl fluoride, 5 mmol/L 2-mercaptoethanol) at 4°C, sonicated at 160 W for 2 min using VCX-400 (Sonics & Materials, Inc., Newtown, CT) at 4°C, and centrifuged at 20,000 × g for 20 min at 4°C to obtain crude protein lysate. HEXIM1 proteins were purified from the crude lysate using ÄKTAprime plus liquid chromatography system equipped with HisTrap HP column (GE Healthcare, Piscataway, NJ), according to the manufacturer's instruction. The purity and quantity of FLAG-His-proteins were examined in 7.5% SDS-polyacrylamide gel electrophoresis followed by Coomassie Brilliant Blue staining.

Western Blotting

Whole cell extracts or tissue extracts from rodents were prepared in RIPA buffer (50 mmol/L Tris-HCl (pH 7.6), 150 mmol/L NaCl, 1% Nonidet-P40, 0.5% sodium deoxycholate, 0.1% SDS) supplemented with 1 mmol/L DTT, 100 nmol/L MG132, protease inhibitor cocktail, and phosphatase inhibitor cocktail as described previously [30]. They were boiled in SDS sample buffer, resolved by SDS-PAGE, and electrically transferred to a PVDF membrane (Millipore, Bedford, MA). Subsequently, Western blotting was performed with appropriate primary antibodies diluted at 1:1000 and horseradish peroxidase-conjugated secondary antibodies (Amersham Biosciences, Buckinghamshire, UK) diluted at 1:2000. Antibody-protein complexes were visualized using the enhanced chemiluminescence method according to the manufacturer's protocol (Amersham Biosciences). Signal intensities of the bands were quantified by using the analysis software Image J from National Institutes of Health.

Immunofluorescence

NRCM were cultured in 6-well plates, and were fixed with 4% paraformaldehyde and permeabilized with phosphate buffered saline containing 0.1% triton-X, and then, blocked with blocking buffer (3% bovine serum albumin and 0.1% Triton-X in Tris-buffered saline). After addition of primary antibodies against alpha-actinin (1:500) or human HEXIM1 (1:1000) for 1 hr at room temperature, the cells were probed with secondary antibodies conjugated with Alexa Fluor 568 (1:500, for alpha-actinin, Invitrogen) and Alexa Fluor 488 (1:500 for HEXIM1, Invitrogen) for 1 hr at room temperature as described previously [15]. The cells were observed by confocal laser scanning microscopy (LSM510; Carl Zeiss, Jena, Germany) with appropriate emission filters. Cardiomyocyte surface area was determined for 400 randomly selected cells in each condition by two blinded observers and quantified using Image J software.

Quantitative RT-PCR (qRT-PCR) Analysis

Total RNA was extracted from cell pellets or crushed tissues using Sepasol-RNA I Super G (Nacalai Tesque) and subjected to reverse-transcription with oligo-dT primers using SuperScript^{T-M}III First-Strand Synthesis System for RT-PCR (Invitrogen). PCR was performed with the LightCycler TaqMan Master, Universal ProbeLibrary Set, and LightCycler® ST300 systems (Roche) according to the manufacturer's instructions as described previously [30]. Expression levels of mRNA were calculated on the basis of standard curves generated for each gene and mRNA for Gapdh was used as an invariant control. The sequences of the primers used in this study are shown below:

For rat,

Gapdh: 5′-agccacatcgctcagaca-3′ and 5′-gcccaatacgaccaaatcc-3′

Nppa (ANP): 5′-caacacagatctgatggatttca-3′ and 5′-cctcatcttc-taccggcatc-3′

Nppb (BNP): 5′-gtcagtcgcttgggctgt-3′ and 5′-cagagctggggaaa-gaagag-3′

Myh7 (beta-MHC): 5′-catcaaggagctcacctacca-3′ and 5′-tcctgcagtcgcagtaggtt-3′

Acta1 (alpha skeletal muscle actin): 5′-tgaagcctcacttcctaccc-3′ and 5′-cgtcacacatggtgtctagtttc-3′

Col1a1 (type I collagen): 5′-catgttcagctttgtggacct-3′ and 5′-gcagctgacttcagggatgt-3′

For mouse,

Gapdh: 5′-agcttgtcatcaacgggaag-3′ and 5′-tttgatgt-tagtggggtctcg-3′

Edn1 (ET-1): 5′-ctgctgttcgtgactttcca-3′ and 5′-agctccggtgct-gagttc-3′

Generation of Cardiomyocyte-specific HEXIM1 Transgenic Mice

The transgene was isolated from the recombinant adenovirus AdCALNL/FHhHEXIM1 described above. The transgenic mice encoding FLAG-His-tagged human HEXIM1 preceded by a floxed stuffer sequence (named loxP-FHhHEXIM1) were generated by pronuclear injection of the transgene into fertilized B6C3F1 oocytes and the founder transgenic mice were crossed into the C57BL/6J genetic background. To create cardiomyocyte-specific HEXIM1 transgenic mice (HEX-Tg), heterozygous loxP-FHhHEXIM1 mice were mated with alphaMHC-Cre mice. All mice were tested and confirmed to be positive for loxP-FHhHEXIM1 and alphaMHC-Cre genes by PCR of genomic DNA from tail tissues. Double transgenic HEX-Tg mice were born at the expected Mendelian ratio, developed normally, and fertile.

Chronic Hypoxia Model of PAH

Adult male wild-type (WT, C57BL/6J) and HEX-Tg mice were randomized to the normoxia or hypoxia group. In hypoxia group, the mice were placed in an airtight chamber with access to food and water ad libitum, and exposed to 10% O_2 using a hypoxic air generator (TEIJIN, Tokyo, Japan) as described previously [32]. Chamber gases were monitored continuously using an O_2 analyzer (JKO-25 SII, JIKO, Japan). After ten weeks of normoxia or hypoxia, the mice were weighed and anesthetized with spontaneous inhalation of isoflurane (Model 400, Univentor, MALTA), and intubated with a mechanical ventilator (Model 28025, UGO BASILE, Italy) on a heating mat (37°C). Left thoracotomy was performed and a 1.4Fr microtip pressure transducer (Micro-Tip Catheter transducer SPR-671, Millar Instruments, Houston Tex) was directly inserted into the RV, and RV systolic pressure (RVSP) was measured with a data acquisition system (ML870 PowerLab8/30 ADInstruments, New South Wales, Australia) when steady state was reached over an interval of at least 10 seconds and averaged as described previously [32]. After completion of hemodynamic measurement, blood samples were collected through cardiac puncture, and the hearts and lungs were excised.

Enzyme-Linked Immunosorbent Assay (ELISA)

Blood samples were centrifuged at 4°C at 500 × g for 15 minutes to separate plasma. Plasma ET-1 levels were measured using ET-1 ELISA kit (Enzo Life Sciences, inc., Farmingdale, NY) according to the manufacturer's directions.

Ultrasound Cardiography

Ultrasound cardiography has done as described previously [32]. Anesthesia was induced with 1.5% isoflurane inhalation and maintained via nosecone, and heart rates were kept between 400–500 beats/min. Noninvasive echocardiographic measurements were performed with a Vevo 2100® (VisualSonics, Toronto, Canada) with a 30-MHz transducer on a heated stage (37°C).

Histopathological Analysis

Formalin-fixed tissues from each animal were cut in paraffin sections (4 μm thick) and mounted onto slides, and Hematoxylin-Eosin and Elastica Van Gieson staining were performed with the right middle lung and heart sections as described previously [32]. The diameters of the cardiomyocytes within the field were measured using standard criteria with Image J software by two blinded operators [33]. A point-to-point perpendicular line was placed across the longitudinally cut myocyte at the level of the nucleus. Transverse or oblique cut myocytes were excluded.

Statistical Analysis

Data were analyzed with Student's t test for unpaired data. P values below 0.05 were considered statistically significant. Graphs represent means ± SD.

Results

Protein Expression of HEXIM1 in the Heart

Previous loss-of-function experiments suggested that the intracellular dosage of HEXIM1 might play a physiological and/or pathophysiological role in the heart, most possibly via determination of cardiomyocyte size and total myocardium volume (See Introduction). In this line, we addressed whether the protein levels of HEXIM1 are variable or not in the heart in physiological contexts. At first, we studied tissue-specific and developmental expression of HEXIM1. As previously reported in mouse heart [34], human heart abundantly expresses HEXIM1, and histological analysis confirmed nuclear localization of HEXIM1 in human cardiomyocytes. Developmentally, HEXIM1 was expressed in the heart from early embryonic stage to fetal periods in mice [22], and gradually decreased after birth (Fig. 1A).

Next, we examined the effects of various cardiovascular drugs on the protein expression of HEXIM1 in NRCM. As previously observed in several cell lines, HMBA significantly induced HEXIM1 expression in cardiomyocytes [19,35,36]. Among others, we found that the eicosanoid vasodilator PGI_2 induced HEXIM1 protein expression in a dose-dependent manner. Whereas, the other drugs used for PAH, ET-1 receptor antagonist BQ123 and PDE-5 inhibitor sildenafil, did not (Figs. 1B and 1C). To confirm the effect of PGI_2 on HEXIM1 protein expression, we studied the cardiac expression of HEXIM1 in PGI synthetase (PGIS)–deficient mice. As shown in Fig. 1D, HEXIM1 levels in $PGIS^{-/-}$ mice were significantly reduced when compared with those in WT mice. Moreover, we revealed that ET-1-induced cellular hypertrophy in NRCM was suppressed by the treatment with PGI_2 and that knockdown of the endogenous HEXIM1 by the expression of siRNA against HEXIM1 significantly cancelled this negative effect of PGI_2 (Fig. 1E). These results indicate that PGI_2 might exert anti-hypertrophic effects on the heart, at least in part, via induction of HEXIM1. Given that PGI_2 has a distinct role in treatment for PAH and exerts an antihypertrophic action in cardiomyocytes [37,38], we decided to test gain-of-function role of HEXIM1 in the heart of PAH.

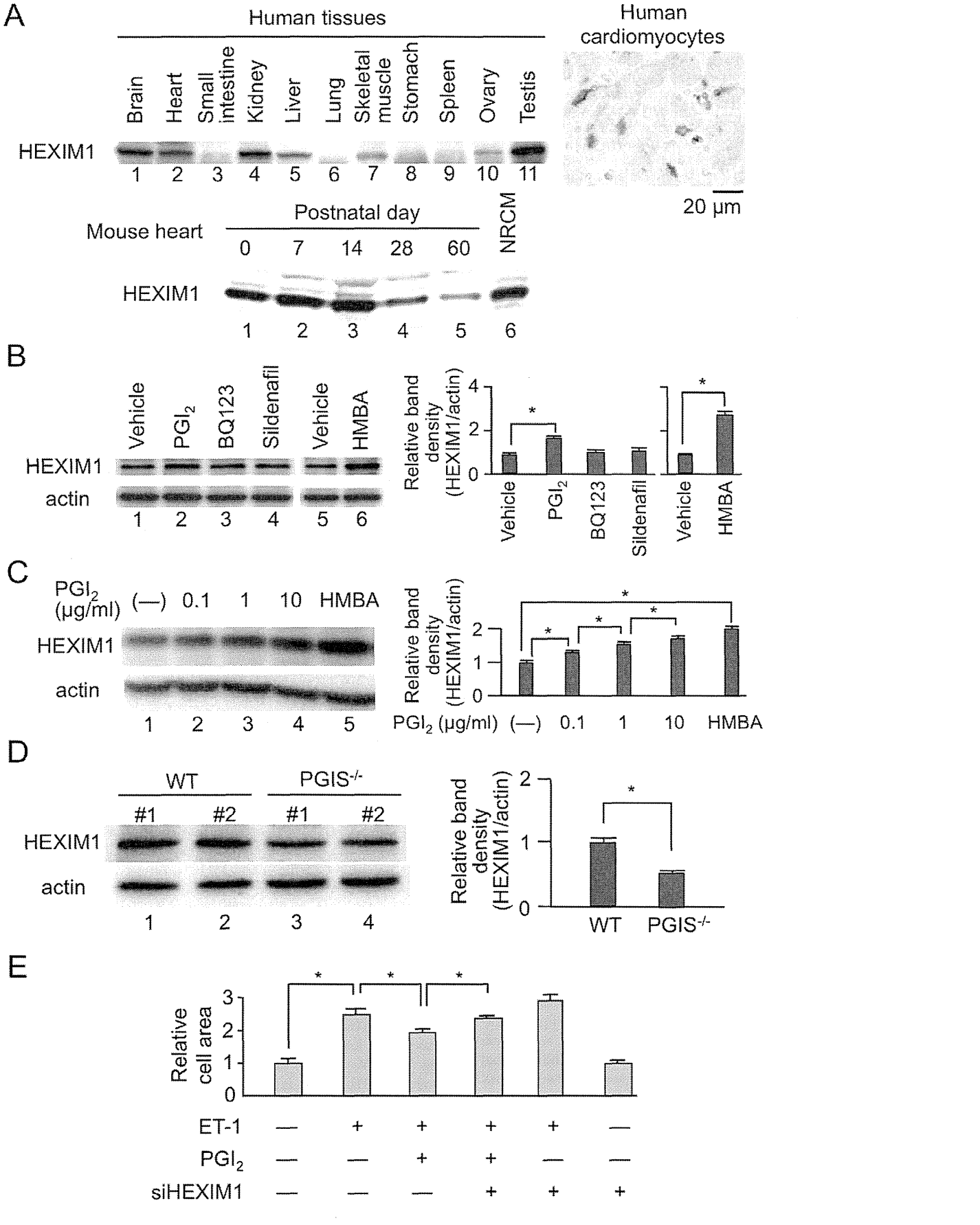
A
Human tissues
Brain
Heart
Small intestine
Kidney
Liver
Lung
Skeletal muscle
Stomach
Spleen
Ovary
Testis
HEXIM1
1 2 3 4 5 6 7 8 9 10 11
Human cardiomyocytes
20 μm
Mouse heart
Postnatal day
0 7 14 28 60
NRCM
HEXIM1
1 2 3 4 5 6
B
Vehicle
PGI2
BQ123
Sildenafil
Vehicle
HMBA
HEXIM1
actin
1 2 3 4 5 6
Relative band density (HEXIM1/actin)
Vehicle
PGI2
BQ123
Sildenafil
Vehicle
HMBA
C
PGI2 (μg/ml) (—) 0.1 1 10 HMBA
HEXIM1
actin
1 2 3 4 5
Relative band density (HEXIM1/actin)
PGI2 (μg/ml) (—) 0.1 1 10 HMBA
D
WT
PGIS-/-
#1 #2 #1 #2
HEXIM1
actin
1 2 3 4
Relative band density (HEXIM1/actin)
WT
PGIS-/-
E
Relative cell area
ET-1 — + + + + —
PGI2 — — + + — —
siHEXIM1 — — — + + +

Figure 1. Protein expression of HEXIM1 in the heart. (A) HEXIM1 protein expression in human tissues and rodent hearts. Twenty micrograms of extracts from different human tissues were subjected to Western blotting (top left). Immunohistochemistry using anti-human HEXIM1 antibodies showed HEXIM1 expression in the nucleus of human cardiomyocytes (top right). The lysates from wild-type (WT) mouse hearts at each time point and neonatal rat cardiomyocytes (NRCM) were subjected to Western blotting for evaluation of postnatal changes of HEXIM1 protein expression in mouse hearts (bottom). (B) Effect of the drugs for treatment of PAH on HEXIM1 protein expression. NRCM were treated with vehicle (water), 1 μg/ml PGI_2, BQ123, sildenafil, or 5 mmol/L hexamethylene bisacetamide (HMBA) for 24 hr, and were analyzed by Western blotting. (C) Effect of PGI_2 on HEXIM1 protein expression. NRCM were treated with vehicle (water), indicated concentration of PGI_2, or 5 mmol/L HMBA for 24 hr, and were analyzed by Western blotting. (D) Decreased expression of HEXIM1 in the heart of PGI synthetase (PGIS) knockout mice. Thirty micrograms of the tissue extracts obtained from the hearts of 24-week-old male WT or PGIS knockout mice ($PGIS^{-/-}$) were subjected to Western blotting. Representative Western blotting of HEXIM1 and actin expression from 5 independent experiments are shown in panels A–D. In panels B–D, the band densities of HEXIM1 detected by Western blotting were quantified and normalized to those of actin. Relative band densities compared to the values obtained from vehicle-treated cells or WT mice are presented (means ± SD, $n=5$). *$P<0.05$. (E) Effect of PGI_2 on endothelin-1 (ET-1)-induced cardiac myocyte hypertrophy. NRCM were infected with control adenovirus Adsictrl or recombinant adenovirus AdsiHEXIM1, which expresses siRNA against HEXIM1, were treated with or without 100 nmol/L ET-1 in the presence or absence of 1 μg/ml PGI_2, and were further cultured for 72 hr. The indirect immunofluorescence for alpha-actinin was performed, the cell area was quantified, and relative cell areas compared to the values obtained from vehicle-treated and Adsictrl-infected cells are presented (means ± SD, $n=400$). *$P<0.05$.
doi:10.1371/journal.pone.0052522.g001

Enhanced Expression of HEXIM1 Prevents ET-1-induced Phosphorylation of RNAPII and Cellular Hypertrophy in Cardiomyocytes via Inhibition of P-TEFb

To address gain-of-function effect of HEXIM1 on cardiomyocytes, we used adenovirus-mediated expression system for HEXIM1 and its mutant (See Materials and Methods) [15]. The mutant HEXIM1, mtHEXIM1, lacks the central domain that mediates suppressive effect on P-TEFb [17]. Since HEXIM1 was supposed to be a negative modulator of P-TEFb and cardiac hypertrophy (See Introduction), we stimulated NRCM with ET-1, a potent inducer of cardiomyocyte hypertrophy [39], and effects of HEXIM1 and mtHEXIM1 were examined. At first, we tested the effect of HEXIM1 on the phosphorylation status of CTD of RNAPII after treatment of NRCM with ET-1. For that purpose, we performed Western blot analysis with the antibodies that recognize either hyperphosphorylated or hypophosphorylated RNAPII (IIo and IIa, respectively). ET-1 treatment increased RNAPII phosphorylation at 15 min (Fig. 2A, compare lanes 1 and 2). Exogenous expression of not mtHEXIM1 but HEXIM1 suppressed this ET-1-induced phosphorylation of RNAPII (Fig. 2A). Ser2 and Ser5 of the CTD heptad repeat are the preferred substrates of Cdk9 and Cdk7, respectively, and ET-1 is shown to preferentially induce phosphorylation at Ser2 [20]. We confirmed this site-specific effect of ET-1 at Ser2 in NRCM, and that not mtHEXIM1 but HEXIM1 suppressed ET-1-triggered phosphorylation at Ser2. In contrast, phosphorylation at Ser5 was not affected by either ET-1 or HEXIM1. There was no significant change in protein levels of Cdk9 and cyclin T1 in the presence or absence of ET-1 treatment and exogenous HEXIM1 (Fig. 2A). Moreover, exogenous expression of not mtHEXIM1 but HEXIM1 counteracted with tropic effect of ET-1 on NRCM size in a multiplicity of infection (MOI)-dependent manner (Fig. 2B). ET-1 binds to the ET receptor on the cell surface and results in activation of the kinase cascade involving, e.g., ERK, JNK, and p38MAPK, and in enhancement of protein synthesis pathway [39,40]. However, exogenous expression of either HEXIM1 or mtHEXIM1 did not significantly affect ET-1-mediated phosphorylation of those kinases and mammalian target of rapamycin (mTOR) activity (Fig. 2C). Collectively, these results indicate that increase in HEXIM1 suppresses ET-1-triggered cell hypertrophy via intervening P-TEFb activation in NRCM.

HEXIM1 Affects ET-1-induced Hypertrophic Gene Expression in Cardiomyocytes

ET-1 stimulation of cardiomyocytes induces expression of several fetal genes, including those for atrial natriuretic peptide (ANP), brain natriuretic peptide (BNP), beta myosin heavy chain (beta-MHC), and alpha skeletal muscle actin [39,41]. Given this, we tested the effect of exogenously expressed HEXIM1 and mtHEXIM1 on those genes expression. ET-1-triggered enhancement of mRNA expression was significantly repressed by HEXIM1 in ANP, BNP, beta-MHC, and alpha skeletal muscle actin genes. The suppressive effect of HEXIM1 was most likely mediated via the central domain, since mtHEXIM1 did not suppress mRNA induction of those genes. On the other hand, mRNA expression of type I collagen was not affected by either type of HEXIM1. In cultured cardiac fibroblasts, HEXIM1 did not significantly affect gene expression of either ANP or type I collagen (Fig. 3). We, therefore, conclude that overexpression of HEXIM1 suppresses ET-1-induced cardiomyocyte hypertrophy in vitro and speculate that negative effects of HEXIM1 on cardiomyocyte growth are caused, at least in part, by repression of fetal gene expression due to P-TEFb suppression in a cardiomyocyte-specific manner.

Cardiomyocyte-specific Overexpression of HEXIM1 Inhibits Progression to RVH in Hypoxia-induced PAH Model

To test in vivo significance of HEXIM1 in PAH, we created the cardiomyocyte-specific transgenic mice for HEXIM1 (HEX-Tg) and those mice were subjected to chronic hypoxia (10% normobaric oxygen for up to 10 weeks) as described in Materials and Methods. In brief, the mice heterozygous encoding FLAG-tagged human HEXIM1 with the loxP–flanked stuffer sequence were crossed with the transgenic mice expressing Cre-recombinase under the control of the alpha-MHC promoter. HEX-Tg mice were generated at predicted Mendelian ratios and survived into adulthood (over 24 months). The appearance and body weight changes of HEX-Tg mice were not different when compared with WT mice (Fig. 4A). We generated a specific antibody against mouse HEXIM1, which does not crossreact with human HEXIM1, to compare expression levels of endogenous HEXIM1 with that of exogenous one (Fig. 4B). Then, we confirmed that exogenous HEXIM1 protein was not expressed in the other tissues, e.g., lung, liver, and skeletal muscle, except for the heart (Fig. 4B). We quantitatively examined the protein levels of exogenous HEXIM1 in HEX-Tg mice; from the comparison with purified recombinant FLAG-tagged human HEXIM1, approximately 3 ng of exogenous FLAG-tagged HEXIM1 were detected per 100 micrograms of tissue extracts from the heart. On the other hand, the protein levels of endogenous HEXIM1 were identical between WT and HEX-Tg mouse heart, and approximately ~5% of exogenous FLAG-tagged HEXIM1 expressed in HEX-Tg mice (Fig. 4C). We also confirmed that both endogenous

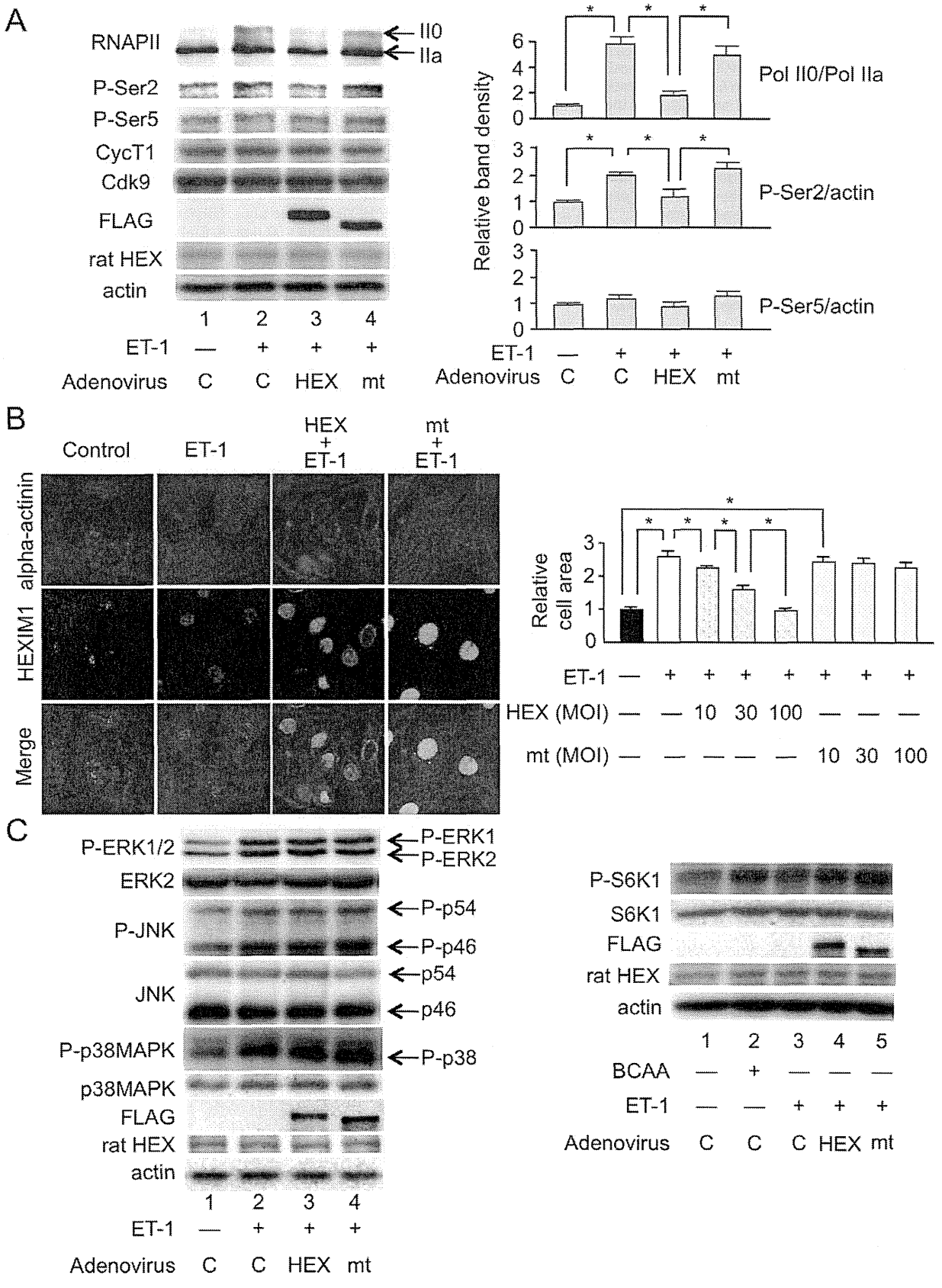

Figure 2. Overexpression of HEXIM1 prevents ET-1-induced phosphorylation of RNA polymerase II and cellular hypertrophy in NRCM. NRCM were infected with irrelevant AxCALNLZ (C) or recombinant adenoviruses, which express FLAG-tagged human HEXIM1 (HEX) or its mutant lacking P-TEFb-binding activity (mt) in the co-presence of Cre recombinase, at MOI of 100 along with Cre recombinase-expressing

recombinant adenovirus and further cultured for 24 hr. (A) Effect of HEXIM1 on the phosphorylation status of the carboxyl-terminal domain (CTD) of RNA polymerase II (RNAPII) after treatment of NRCM with ET-1. The cells were treated with or without 100 nmol/L ET-1 for 15 min. Expression and phosphorylation levels of RNAPII were analyzed by Western blotting. *Left*, representative images of Western blotting of hyper- (IIO) and hypo- (IIa) phosphorylated RNAPII, phosphoserine 2 (P-Ser2), phosphoserine 5 (P-Ser5), cyclin T1 (CycT1), Cdk9, exogenous and endogenous HEXIM1 (FLAG and rat HEX, respectively), and actin expression from 5 independent experiments are shown. *Right*, band densities of IIO, and P-Ser2 and P-Ser5 detected by Western blotting were quantified and normalized to those of IIa and actin, respectively, and relative band densities compared to the values obtained from control cells (AxCALNLZ-infected and vehicle-treated cells) are presented in the right panel (means ± SD, n = 5). *P<0.05. (B) Effect of HEXIM1 on hypertrophic cell growth in response to ET-1 in NRCM. The cells were treated with or without 100 nmol/L ET-1 and further cultured for 72 hr. *Left*, indirect immunofluorescence was performed. Alpha-actinin and HEXIM1 are shown in red and green, respectively. Representative fluorescent microscopic images from 5 independent experiments are shown. *Right*, recombinant adenoviruses were infected at indicated amount. The indirect immunofluorescence for alpha-actinin was performed, the cell area was quantified, and relative cell areas compared to the values obtained from vehicle-treated cells are presented (means ± SD, n = 400). *P<0.05. (C) Effect of HEXIM1 on the phosphorylation status of ERK1/2 and MAP kinases, and mTOR activity in response to ET-1 in NRCM. *Left*, the cells were treated with or without 100 nmol/L ET-1 and further cultured for 1 hr. *Right*, the medium was replaced to amino acid-deprived DMEM, and the cells were treated with or without 100 nmol/L ET-1 in the presence or absence of 10 mmol/L BCAA cocktail and further cultured for 1 hr. Expression and phosphorylation levels of ERK1/2, JNK (p54 and p46), p38MAPK, S6K1, exogenous and endogenous HEXIM1 (FLAG and rat HEX, respectively), and actin were analyzed by Western blotting. Representative images of Western blotting from 5 independent experiments are shown.
doi:10.1371/journal.pone.0052522.g002

and exogenous HEXIM1 levels appeared not to be affected after hypoxia exposure in both mice (Fig. 4C).

In PAH model after chronic hypoxia exposure, the pathology of the pulmonary vasculature was grossly typical as reported [42,43], including, e.g., medial thickening and muscularization of small arteries in the alveolar walls, and the increase of collagen fibers both in WT and HEX-Tg mice. The extent of elevation in RV systolic pressure, plasma concentrations and mRNA expression in the lungs of ET-1, were also similar (Fig. 5). We, therefore, concluded that PAH was similarly generated in both mice. Concerning cardiac phenotype, however, the degree of RVH was less marked in HEX-Tg mice compared with WT mice; the RV weight to left ventricular (LV) and septum weight ratio (RV/(LV+S)) and RV weight to body weight ratio (RV/BW) were not significantly increased in HEX-Tg mice. LV+S weight to BW ratio ((LV+S)/BW) was comparable between WT and HEX-Tg mice (Fig. 6A). In WT mice, the diameter of cardiomyocytes in RV wall were significantly increased under exposure to chronic hypoxia, supporting the previous notion that afterload-driven RVH is due not to increased in the number of myocytes but to the increased cell size [5]. In clear contrast, HEX-Tg mice did not show significant enlargement of myofiber diameter (Fig. 6B). We evaluated RV function by cardiac ultrasonography and revealed significant RV dilatation not in HEX-Tg mice but solely in WT mice. Under this condition, left ventricular ejection fraction (LV%EF) was not impaired in either mouse (Fig. 6C).

Taken together, these findings indicated that cardiomyocyte-specific overexpression of HEXIM1 inhibits progression to RVH under chronic hypoxia, most possibly via inhibition of P-TEFb-mediated enlargement of cardiomyocytes.

Discussion

In the fetus, cardiovascular physiology is characterized by a high-resistance pulmonary circulation and low-resistance systemic circulation. After birth and in infancy, RVH regresses and the heart remodels to the typical postnatal heart with a crescent-shaped RV and elliptic LV [2,44]. Interestingly, HEXIM1 is highly expressed in the fetus and early postnatal period [22] and its expression is gradually decreased (Fig. 1). Considering that HEXIM1 might possess negative effect on cardiomyocyte growth, it is likely that this developmental stage-dependent alteration in HEXIM1 expression levels may be associated with physiological cardiovascular development. In addition, we showed that PGI_2, a therapeutic drug for PAH,

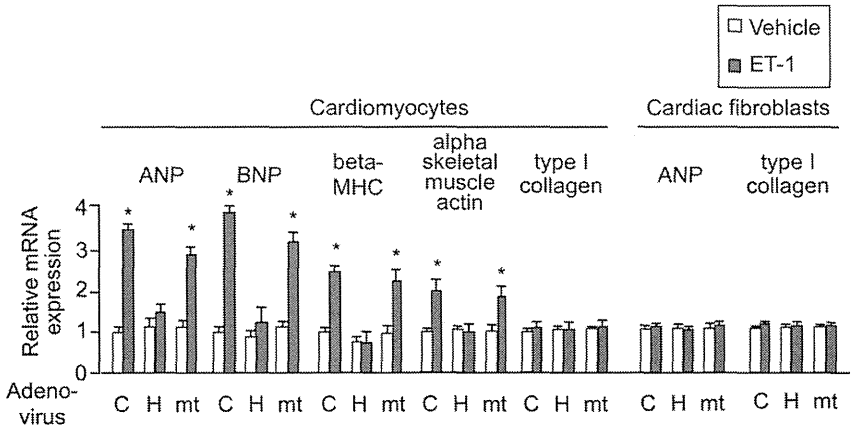

Figure 3. Overexpression of HEXIM1 prevents ET-1-induced mRNA expression of cardiac hypertrophic genes in NRCM. NRCM or cardiac fibroblasts were infected with irrelevant AxCALNLZ (C) or recombinant adenoviruses, which express FLAG-tagged human HEXIM1 (HEX) or its mutant lacking P-TEFb-binding activity (mt) in the co-presence of Cre recombinase, along with Cre recombinase-expressing recombinant adenovirus. After 24 hr, the cells were treated with vehicle or 100 nmol/L ET-1 and further cultured for 24 hr. Total RNA was extracted from the cells and expression levels of indicated mRNA were assessed in qRT-PCR analysis. Results were normalized to GAPDH mRNA levels and are shown as relative mRNA expression to expression levels in the control cells (AxCALNLZ-infected and vehicle-treated cells). Error bars represent SD (n = 5). *P<0.05 vs. vehicle-treated cells.
doi:10.1371/journal.pone.0052522.g003